J MATER RES TECHNOL. 2016;xxx(xx):xxx–xxx

Available online at www.sciencedirect.com

jmr&t Journal of Materials Research and Technology

www.jmrt.com.br

Original Article

Wear resistance enhancement of titanium alloy (Ti–6Al–4V) by ball burnishing process

Goutam Devaraya Revankar[a,*], *Raviraj Shetty*[b], *Shrikantha Srinivas Rao*[c], *Vinayak Neelakanth Gaitonde*[d]

[a] *Department of Mechanical Engineering, Tontadarya College of Engineering, Gadag, India*
[b] *Department of Mechanical and Manufacturing Engineering, Manipal Institute of Technology, Manipal, India*
[c] *Department of Mechanical Engineering, National Institute of Technology Karnataka, Surathkal, India*
[d] *Department of Industrial and Production Engineering, B.V.B. College of Engineering and Technology, Hubli, Karnataka, India*

ARTICLE INFO

Article history:
Received 21 July 2015
Accepted 30 March 2016
Available online xxx

Keywords:
Titanium alloy (Ti–6Al–4V)
Taguchi technique
Ball burnishing
Wear rate
Coefficient of friction

ABSTRACT

The objective of the research was to improve the wear resistance of titanium alloys by ball burnishing process. Burnishing process parameters such as burnishing speed, burnishing feed, burnishing force and number of pass were considered to minimize the specific wear rate and coefficient of friction. Taguchi optimization results revealed that burnishing force and number of pass were the significant parameters for minimizing the specific wear rate, whereas the burnishing feed and speed play important roles in minimizing the coefficient of friction. After burnishing surface microhardness increased from 340 to 405 Hv, surface roughness decreased from 0.45 to 0.12 μm and compressive residual stress were generated immediately below the burnished surface. The optimization results showed that specific wear rate decreased by 52%, whereas coefficient of friction was reduced by 64% as compared to the turned surface. The results confirm that, an improvement in the wear resistance of Ti–6Al–4V alloy has been achieved by the process of ball burnishing.

1. Introduction

Titanium alloys are of an increasing importance in engineering applications because of their excellent combination of high strength, low density and corrosion resistance. Titanium alloy finds wide applications in aerospace, automotive, nuclear, chemical, marine and biomedical industries. Ti–6Al–4V alloy is a widely applied titanium alloy that alone covers about half of the total world production of titanium alloys [1]. However, Ti–6Al–4V alloy is known to possess poor wear resistance that restricts its applications particularly in areas involving wear and friction [2,3]. The scope of the applications for titanium alloys has been somewhat impeded owing to poor wear resistance under abrasion and erosion conditions [2,4–6]. Molinari et al. [7] studied the dry sliding wear behavior of Ti–6Al–4V alloy sliding against itself at different sliding velocities and applied loads

* *Corresponding author.*
E-mail: goutamdr@gmail.com (G.D. Revankar).
http://dx.doi.org/10.1016/j.jmrt.2016.03.007

Please cite this article in press as: Revankar GD, et al. Wear resistance enhancement of titanium alloy (Ti–6Al–4V) by ball burnishing process. J Mater Res Technol. 2016. http://dx.doi.org/10.1016/j.jmrt.2016.03.007

to confirm the low wear resistance of the alloy to plastic deformation at low loads and poor protection exerted by the surface oxide. The dominant reason for the poor wear resistance of Ti–6Al–4V alloy is due to low protection exerted by the tribooxides. The tribolayer of Ti–6Al–4V alloy is brittle, tended to be continuously fragmented and did not adhere to the substrate, thus presenting no protective role [7,8]. Alam Ohidul and Haseeb [9] investigated the tribological properties of Ti–6Al–4V and Ti–24Al–11Nb alloys subjected to dry sliding wear against hardened-steel and found that the lower wear rate of Ti–6Al–4Valloy alloy was linked to severe delamination wear. An unexpectedly high wear rate for alumina sliding against Ti–6Al–4V (pin on-disk tests) was reported by Dong and Bell [10]. Qiu et al. [11] investigated tribological characteristics of Ti–6Al–4V alloy against GCr15 under high speed and dry sliding and concluded that the low wear resistance of Ti–6Al–4V alloy was attributed to the formation of a loosened oxide layer. Magaziner et al. [12] studied wear behavior of Ti–6Al–4V under reciprocation sliding conditions and observed that the wear loss was due to the adhesion and abrasion mechanism without citing the effect of tribooxides.

A familiar approach for enhancing the tribological properties of titanium alloys for improved wear resistance is to perform surface modifications for increased hardness and reduction in friction coefficient [13–15]. Surface treatment is the suitable solution for the elevation of the wear resistance of Ti–6Al–4V. Thermal oxidation is a popular process which substantially improves the wear resistance [16,17]. A few of these procedures applied are PVD coating (TiN, TiC), ion implantation (N^+), thermal treatments (nitriding, diffusion hardening) [18], or laser alloying with TiC [19]. However, these procedures have limited technical success for example ion implantation leads to modification of only a thin layer (>10 μm), resulting in the improvement in the sliding wear resistance of Ti–6Al–4V. But this treated surface wears away or becomes discontinuous, promoting catastrophic wear. Surface modification by oxygen diffusion hardening (ODH) has been considered to enhance the wear resistance of Ti–6Al–7Nb, due to a gradual increase in hardness through a relatively thick transformed layer [20]. A similar approach was taken by Zwicker et al. [21] for enhanced friction behavior of Ti–5Al–2.5Fe against UHMWPE, using oxide films formation by thermal oxidation. Johnson et al. [14] applied a low-cost approach of thermal oxidation to modify Ti–6Al–4V surfaces and achieved friction coefficients as low as 0.1, i.e. a reduction of 70% in comparison to the untreated alloy. The thermal processes such as nitriding [22], carburization [23], boriding [24] and thermal plasma coating techniques [25] used for surface treatment have a limitation that the high thermal stresses produced lead to torsional twisting of substrates resulting in surface roughening. Efforts to enhance the tribological performance of Ti–6Al–4V using SiC or B_4C coatings alone failed as there was no significant improvement on wear performance, despite a noticeable increase in surface hardness [26]. The process of shot peening was employed, which led to an improvement in the wear resistance due to surface hardening of Titanium alloy Ti–6Al–4V, but also resulted in, increase in surface roughness [27].

Burnishing is an acknowledged method of mechanical surface treatment, to impart specific physical, mechanical and tribological properties. Burnishing process is a post-machining operation in which the surface of the work piece is compressed by the application of a ball or roller to produce a smooth and work-hardened surface by plastic deformation of surface irregularities. Burnishing process is capable of improving the resistance to wear, corrosion and oxidation. These improvements can be extended to minimize friction and reduce adhesion. Many investigators have pointed out that burnishing reduces friction coefficient and improves wear resistance. From the experimental trials conducted on burnishing of copper, El-Tayeb [28], revealed that burnishing process helps to reduce friction up to a critical depth, beyond which cracks are initiated resulting in increase of friction coefficient. El-Tayeb and Ghobrial [29] found that burnishing process reduced wear rate by 38% for copper and 44% for St-37 steel, whereas an increase in burnishing depth accelerated the response for wear rate resulting in surface damage. El-Tayeb et al. [30] in their study on burnishing of Aluminum 6061 proved that ball burnishing process is capable of improving friction coefficient by 48% reduction and weight loss by 60–80% reduction. Rao et al. [31] studied the effects of burnishing parameters on the surface hardness and wear resistance of HSLA dual phase steel alloys and observed that the percentage reduction in weight of the components decreases with increase in burnishing force. Rajasekariah and Vaidyanathan [32] conducted burnishing trials on steel components and observed an increase in wear-resistance of 40% due to burnishing. Low and Wong [33] conducted ball burnishing on polymers under dry sliding conditions and determined that the lowest coefficient of friction value achieved was 0.22 (32.9% decrease) for polyoxymethylene (POM) and 0.24 (28.8% decrease) for polyurethane (PUR), whereas the lowest specific wear rate value achieved was 0.31×10^{-6} mm^3/N m (38.6% decrease) for polyoxymethylene (POM) and 0.41×10^{-6} mm^3/N m (37.9% decrease) for polyurethane (PUR).

From the earlier investigations, it is evident that the final effect of smoothing during burnishing process depended profoundly on the initial roughness [34,35]. Feng et al. [36] carried out turning and burnishing trials on aluminum alloys AA 7075 and AISI 5140 and revealed that lowest surface roughness after burnishing is proportional to the initial surface roughness. Titanium alloy (Ti–6Al–4V) is classified as difficult to machine material. Hence, understanding the machining characteristic of titanium alloy and determining the finish cutting parameters is important. The turning process has to be carried out to identify the optimal condition of process parameters to obtain best surface finish. In the present scenario, the use of flood cutting fluids in machining processes has been criticized largely due to the several negative effects on environment and health. Extensive attention has been given to reduce or completely eliminate the use of cutting fluids and meet the demands for environment friendly cutting processes. One such alternative in this regards is the application of minimum quantity lubrication (MQL) to obtain best surface finish. From the works of Radoslaw et al. [37] it is proved that application of the minimum quantity cooling lubrication (MQCL) and MQL method reduces the values of roughness parameters of machined surface of X10CrNi18-8 stainless steel as compared to dry machining. The analysis and directions of MQCL adjustment trends needed to improve the machining

Please cite this article in press as: Revankar GD, et al. Wear resistance enhancement of titanium alloy (Ti–6Al–4V) by ball burnishing process. J Mater Res Technol. 2016. http://dx.doi.org/10.1016/j.jmrt.2016.03.007

performance are presented in the work of Radoslaw et al. [38]. The investigation of the technological parameters affecting microhardness after turning duplex stainless steel (DSS) with wedges of coated sintered carbide for different cutting conditions was carried out by Krolczyk et al. [39].

Burnishing is a highly nonlinear problem, in which local large strain/deformation, as well as material nonlinearities and unknown boundary conditions in contact area are involved. The models in the field of burnishing can be classified into three categories namely analytical [36,40,41], statistical [42] and FE models [43]. Skalski et al. [43] studied the burnishing indentation process of burnishing ball into workpiece using axisymmetric FEM to analyze the relations between contact pressure, plastic strain depth and burnishing force. Röttger [44] developed a 2D plane strain FEM model for analysis of ball burnishing on the hardened steel using DEFORM-2D. The predicted surface finish (R_a) and residual stresses of the FEM model agreed reasonably with the experimental values. Bouzid et al. [40] investigated the effects of burnishing on the surface roughness of AISI 1042 steel and developed an analytical model to analyze the surface roughness after burnishing. Beres et al. [45] used 2D and 3D finite element method to model the LPB process numerically. Bouzid and Sai [46] developed a 3D FEM model of the burnishing indentation process to analyze the residual stress induced during burnishing. A reliable FE model of burnishing process was also presented by Sartkulvanich et al. [47]. They developed a more accurate 2D and 3D FEM models to analyze the influence of burnishing parameters on surface roughness and residual stress based on Rottger's [44] work. Bougharriou et al. [48] developed an analytical model and a finite element model to provide a fundamental understanding of the burnishing process on an AISI 1042 material. Maximov and Duncheva [49] analyzed ball burnishing process of low alloy steel by 2D FEM using software ABAQUS/Implicit. The results obtained by these authors demonstrate that finite element models were able to predict the effect of burnishing process parameters on the residual stress distributions successfully, when compared with experimental data.

The aim of the present work is to investigate the wear resistance of turned and burnished titanium alloy specimens using the pin-on-disk testing in accordance with the ASTM G99-95 standard. Further, a finite element model of the process is presented, showing its useful application for the study of the residual stresses generated and the experimental values are compared with simulated one.

2. Experimental details

12 mm diameter bars of titanium alloy (Ti–6Al–4V) were used as work materials. Titanium alloy, Ti–6Al–4V work material is a ($\alpha+\beta$) alloy of aerospace Grade 5, whose chemical composition of the work material is specified in Table 1. The turning and burnishing tests were performed on '*Ace Turn mill CNC Fanuc lathe*' of 11 kW spindle power with a maximum spindle speed of 4000 rpm. From the initial turning experiments conducted by the authors, the titanium bars were turned to proper dimensions, i.e., 12 mm diameter using poly crystalline diamond (ISO designation of CCMT09T304) tool under MQL conditions with a flow rate of 150 ml/h, speed of 150 m/min and a feed of 0.15 mm/rev [50]. The work pieces were prepared with one recess such that each work piece could be used for two different burnishing conditions. The microstructure of the α- and β-phase on the cross sections of the titanium alloy Ti–6Al–4V is shown in Fig. 1. After turning the average roughness and hardness obtained were in the range from 0.40 to 0.45 μm (R_a) and 340 (Hv), respectively.

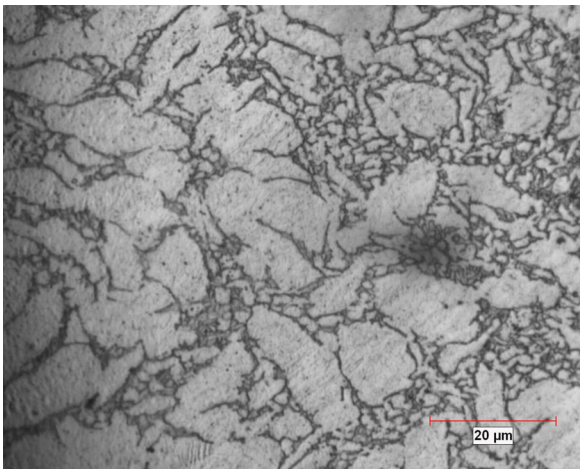

Fig. 1 – Microstructure of titanium specimen.

In the present study, four parameters, namely, burnishing speed, burnishing feed, burnishing force and number of passes were identified and the range for each of the process parameters was determined through the preliminary experiments [51]. Each process parameter was investigated at three levels to study the non-linearity effects of process parameters. The identified process parameters and their levels in the current investigation of burnishing process are summarized in Table 2. According to Taguchi design concept, L_9 orthogonal array (OA) with 4 columns and 9 rows was selected [52,53]. Each burnishing process parameter is assigned to a column and nine different process parameter combinations are available. Thus, nine experiments are required to study the complete burnishing process parameter space using L_9 OA. The experimental layout for the current investigation using L_9 OA as shown in Table 3.

Table 1 – Chemical composition of titanium alloy (Ti–6Al–4V) used in the current investigation.

	Element								
	Ti	Al	V	Fe	O	C	N	Y	H
wt.%	Balanced	6.1	4	0.16	0.11	0.02	0.01	0.001	0.001

Please cite this article in press as: Revankar GD, et al. Wear resistance enhancement of titanium alloy (Ti–6Al–4V) by ball burnishing process. J Mater Res Technol. 2016. http://dx.doi.org/10.1016/j.jmrt.2016.03.007

Table 2 – Ball burnishing process parameters and their identified levels.

Code	Parameter	Levels		
		1	2	3
A	Speed (m/min)	15	30	45
B	Feed (mm/rev)	0.05	0.10	0.15
C	Force (N)	150	200	250
D	No. of passes	1	2	3

In the present study, external ball burnishing tests were performed under lubricated conditions using SAE 40 oil, as per the experimental plan of Table 3. A specially designed innovative ball-burnishing tool, which consists of two steel parts, was employed. The first part of square cross section is a shank held on the lathe tool post, whereas the other part is a mandrel of material EN 31 to hold both the active ball (8 mm in diameter) made of carbide. The ball holder that is the mandrel was elastically supported by a helical spring. This ball is further supported by three small carbide balls of 4 mm diameter. The sectional view of the ball burnishing tool is shown in Fig. 2. With this arrangement the active ball was free to rotate with the rotation of the work piece when the active ball is set in contact with the surface of the work piece, during burnishing process due to the frictional forces developed. The ball could be removed easily from the tool for changing, readjusting or cleaning by unscrewing the cage. The movement of the mandrel due to the applied burnishing force will cause compression of the spring. This compression has been calibrated to measure the burnishing force. The burnishing force is measured with help of spring of known stiffness and dial gauge. Keeping the spring inside the tool and placing the dial gauge at the end of the tool shank, the deflection of dial gauge is noted down for determining the burnishing force. Normally, the optimum burnishing force varies between 200 and 500 N depending on the type of alloys. Increase in burnishing force is unadvisable, because it increases the surface roughness, mainly due to the distortion of the microprofile and excessive work hardening. In the present investigation, the burnishing tool has been designed for the maximum permissible force of 400 N. Our preliminary investigation revealed that high forces cause shear failure in the subsurface layers, which in turn caused flaking. Taking into considerations of these, the burnishing force is varied from 150 to 250 N. Because surface finish gets deteriorated due to hard particles, which usually leave deep scratches, alcohol was used as a precautionary step to clean the work piece surface before burnishing, i.e., after turning in order to prevent hard particles entering the contact surface between the tool and the work piece. The specimens were also cleaned with alcohol before the response tests to measure surface roughness and hardness.

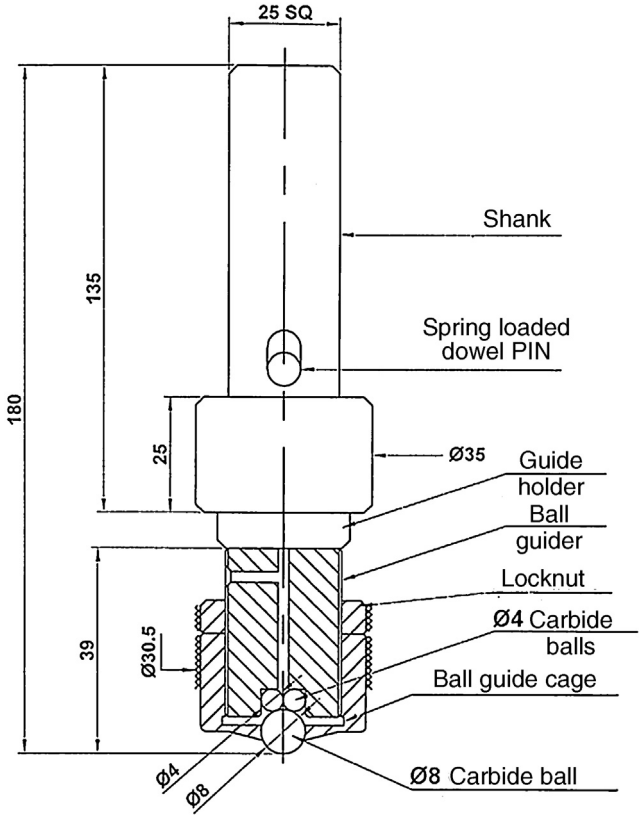

Fig. 2 – Sectional view of ball burnishing tool.

The surface roughness of the turned and burnished surfaces was measured with a portable '*Mitutoyo Surftest SJ-400*' surface roughness instrument. All the measurements were carried out with a cutoff length of 0.8 mm and in each case the average of five readings was used. The surface roughness was measured to assess the quality of the burnished surface quantitatively. The hardness was measured using computerized microvickers hardness testing machine (*Model VM50 50PC*). The surface hardness of each specimen was measured along the length and around the periphery. The average values of three measurements for each specimen were recorded. The measured values of surface roughness and hardness are summarized in Table 3. After turning and burnishing, cylindrical specimen of 12 mm diameter and 5 mm thickness for each trial were cut using the wire electro discharge machine Electronica (Maxicut). Wire EDM was used because it is relatively fast simple and accurate way of removing specimen from the machined bars without further inducing unwanted residual stresses in the surface.

Wear tests were conducted, on a pin-on-disk wear testing machine (Model: TR-20, DUCOM) as per ASTM: G99-95 [54]. The counterpart disk was made of quenched and tempered EN-32 steel having a surface hardness of 65HRC and surface roughness $R_a = 1.60\ \mu m$. The cylindrical wear specimens of size Ø12 × 5 mm thickness cut from the turned and burnished bar, were clamped in such a way that the burnished surface comes in contact with the counterpart disk. The specimens were cleaned with acetone before conducting the test. The wear tests were conducted under dry sliding condition at a constant load of 10 N, with a sliding velocity of 2.68 m/s and a

Please cite this article in press as: Revankar GD, et al. Wear resistance enhancement of titanium alloy (Ti–6Al–4V) by ball burnishing process. J Mater Res Technol. 2016. http://dx.doi.org/10.1016/j.jmrt.2016.03.007

Table 3 – Orthogonal array, measured responses and corresponding S/N ratios.

Tr. no.	Speed	Feed	Force	No. of pass	Hardness (Hv)	S/N ratio for hardness (dB)	Surface roughness (μm)	S/N ratio for surface roughness (dB)	Specific wear rate, W_r ($\times 10^{-4}$ mm^3/N m)	S/N ratio for specific wear rate (dB)	Coefficient of friction	S/N ratio for coefficient of friction (dB)
1	1	1	1	1	378	51.5498	0.13	17.7211	4.72621	66.5097	0.20	13.9794
2	1	2	2	2	371	51.3875	0.16	15.9176	4.97496	66.0642	0.21	13.5556
3	1	3	3	3	405	52.1491	0.27	11.3727	3.31664	69.5860	0.32	9.8970
4	2	1	2	3	400	52.0412	0.12	18.4164	3.77268	68.4670	0.19	14.4249
5	2	2	3	1	395	51.9319	0.23	12.7654	3.95924	68.0478	0.25	12.0412
6	2	3	1	2	388	51.7766	0.25	12.0412	4.51892	66.8993	0.28	11.0568
7	3	1	3	2	398	51.9977	0.19	14.4249	3.91778	68.1392	0.24	12.3958
8	3	2	1	3	385	51.7092	0.18	14.8945	4.85059	66.2841	0.27	11.3727
9	3	3	2	1	382	51.6413	0.26	11.7005	4.74694	66.4717	0.31	10.1728

Please cite this article in press as: Revankar GD, et al. Wear resistance enhancement of titanium alloy (Ti–6Al–4V) by ball burnishing process. J Mater Res Technol. 2016. http://dx.doi.org/10.1016/j.jmrt.2016.03.007

Table 4 – Parameters for friction and wear test.

Parameter	Value
Sliding velocity (m/s)	2.68
Test duration (s)	180
Load (N)	10
Lubrication	Dry

constant sliding time of 180s as shown in Table 4. All the tests were conducted in ambient air conditions with temperature and humidity in the range of 18–22 °C and 52–62%, respectively [55]. The data reflected the average value and standard deviation of 3 wear tests. Good repeatability was obtained in both friction and wear results. An electronic balance with an accuracy of 0.01 mg was used to measure the mass loss of the pin specimen for the evaluation of wear. At the end of each test, the specimen was weighed again on the same balance after cleaning with acetone. To measure slide mass loss, the difference between the initial and final weights was taken and was divided by the sliding distance to calculate the wear rate. Mass based wear rate was then converted to volumetric wear rate using the density of the titanium alloy (0.00451 g/mm^3).

The specific wear rate, W_r (mm^3/N m) was calculated using Eq. (1)

$$W_r = \frac{\Delta m}{\rho t V_s F_N} \tag{1}$$

where, Δm is the mass loss on the pin samples (g), ρ is the density of the test sample (g/mm^3), t is the test duration (s), V_s is the sliding velocity (m/s), F_N is the average normal load (N).

The friction force was monitored by a load cell-based force measurement system. The microstructure of the turned and burnished surface of titanium work-piece was obtained for each sample by using scanning electron microscope. The microstructure of each turned and burnished sample at other magnifications were also obtained in order to perform a detailed study. The residual stresses of turned and burnished parts were measured by X-ray diffraction method. The SEM is operated at an acceleration voltage of 10–30 kV. For examination by optical microscope or in SEM by SE-signal mode, polished samples were submerged in Kroll's reagent for 15 s. After etching, they were immediately rinsed in ethanol and then water. The Kroll's reagent with composition 92 ml distilled water, 6 ml nitric acid and 2 ml HF was used as macro- and microetchant. After mechanical polishing and etching for some specimen, thorough rinsing in ultrasonic acetone bath was performed. Samples were then flushed with ethanol. All the samples were cleaned in plasma cleaner as a final step, before insertion into SEM. Samples were handled with rubber gloves after this final cleaning stage. The sample was prepared by electro polishing to carry out EBSD analysis and X-ray diffraction method. The viable option to obtain deep measurements was electro-polishing, as other methods could change the stress state of the piece. To carry out the process of electro polishing, three operations were carried out, metal preparation, electro polishing and post treatment. The instrument Struers Electropol was used for electro polishing. The paper of 400, 1000, 2500 Grade were used for diamond polishing with 1 micron diamond paste. The electro-polishing solution used was an equal volume mixture of 80% mass fraction methanol and 20% percloric acid solution. The operating conditions were current densities of 15 V and operation time is of 45 s.

Table 5 – ANOM for specific wear rate based on S/N ratio.

Parameter code	Levels			Optimum level
	1	2	3	
A	67.3867	67.8047	66.9650	**2**
B	67.7053	66.7987	67.6524	**1**
C	66.5644	67.0010	68.5910	**3**
D	67.0097	67.0342	68.1124	**3**

Bold indicates optimum levels of the process parameters.

The worn surfaces after wear testing were examined under Scanning Electron Microscopy. Electron back-scattered diffraction (EBSD) analyses were performed on turned and burnished specimens. Automatic generation and indexing of EBSD patterns were carried out on SEM of FEI Company produced by TSL Technology Inc., which contained a back-scattered electron detector and OIM software (Version-7.O.1) for analysis. The experimental software used is TSL OIM data collection. Beam scan mode was adapted with a step spacing of 0.8 mm. The image of microstructure was reconstructed by creating grain boundary maps from the EBSD pattern measurements.

3. Results and discussion

3.1. ANOM and ANOVA

In the present work, the objective is to minimize the specific wear rate and coefficient of friction during burnishing process. Hence, "smaller the better type" category for the specific wear rate (W_r) and coefficient of friction (μ) has been selected. Moreover, to study the effect of burnishing parameters on hardness (H) and surface roughness (R_a), "larger the better type" category for hardness and "smaller the better type" category for surface roughness have been selected The S/N ratio associated with the objective functions for each trial of the orthogonal array is given by:

$$\eta_1 = -10\log_{10}(Wr^2) \tag{2}$$

$$\eta_2 = -10\log_{10}(\mu^2) \tag{3}$$

$$\eta_4 = -10\log_{10}(Ra^2) \tag{4}$$

$$\eta_3 = -10\log_{10}(H^{-2}) \tag{5}$$

The corresponding S/N ratios for each trial of L_9 orthogonal array were determined using Eq. (2) to Eq. (5) and are presented in Table 3. The analysis of means (ANOM) based on S/N ratio was carried out to determine the optimal levels of process parameters. The results of ANOM for specific wear rate and coefficient of friction are represented in Tables 5 and 6, respectively. The level of a parameter with the highest value of S/N ratio is the best combination level. The optimal parameter setting is found to be *A2*, *B1*, *C3* and *D3* for minimum specific

Please cite this article in press as: Revankar GD, et al. Wear resistance enhancement of titanium alloy (Ti–6Al–4V) by ball burnishing process. J Mater Res Technol. 2016. http://dx.doi.org/10.1016/j.jmrt.2016.03.007

Table 6 – ANOM for coefficient of friction based on S/N ratio.

Factor code	Levels			Optimum level
	1	2	3	
A	12.4773	12.5077	11.3138	**2**
B	13.6000	12.3232	10.3755	**1**
C	12.1363	12.7178	11.4447	**2**
D	12.0645	12.3361	11.8982	**2**

Bold indicates optimum levels of the process parameters.

wear rate and the optimal parameter setting for minimum coefficient of friction is found to be *A2*, *B1*, *C2* and *D2*.

To investigate the effects of burnishing process parameters quantitatively, the analysis of variance (ANOVA) based on S/N ratio has been employed [52,53]. Table 7 gives the summary of ANOVA results of specific wear rate. It can be seen from the ANOVA tables that the burnishing force (57.77%) and number of passes (20.13%) play major roles in minimizing the specific wear rate, whereas burnishing speed (13.15%) and burnishing feed (8.95%) do not show noticeable effects in controlling the specific wear rate. Similarly, Table 8 gives the summary of ANOVA results of coefficient of friction. It can be seen from the ANOVA tables that the burnishing feed (74.17%) and burnishing speed (13.03%) play major roles in minimizing the coefficient of friction, whereas burnishing force (11.43%) and number of passes (1.37%) do not show noticeable effects in controlling the coefficient of friction.

Here, the best combination values of the process parameters obtained through Taguchi optimization were set and the work pieces of the same batches were machined. The observed value of S/N ratio (η_{obs}) is compared with that of the predicted value (η_{opt}). Table 9 gives the confirmatory test results and it is observed from the table that the prediction error, i.e., ($\eta_{opt} - \eta_{obs}$) is permissible. The best combinations of process parameters for optimum specific wear rate and coefficient of friction, along with the corresponding optimal values are given in Table 10.

Table 9 – Results of confirmatory tests.

Performance measure	Specific wear rate	Coefficient of friction
Levels, A, B, C, D	2, 1, 3, 3	2, 1, 2, 2
S/N predicted, η_{opt} (dB)	69.6378	14.6263
Observed value	0.000329 $mm^3/N\,m$	0.1856
S/N observed, η_{obs} (dB)	69.6561	14.6284
Prediction error (dB)	−0.0183	−0.0021
Confidence interval value, CI (dB)	±3.7601	±1.9797

3.2. *Analysis of hardness*

Due to the application of high burnishing force to the material surface, a localized cold worked zone is created leading to plastic deformation, which creates a localized cold worked layer. This layer provides a corrosion resistance enhancement and also a wear resistance improvement of sliding component [15]. It is evident from the findings of Table 3 that the hardness of the burnished specimen was in the range of 371–405 Hv as compared to the turned specimen whose hardness was recorded as 340 Hv. The microhardness depth distribution of titanium material for Trial no.6 as per the experimental plan (Table 3), after burnishing is shown in Fig. 3. The hardness value of the surface is much higher than the bulk material hardness. At 250 μm beneath the burnished surface, the difference in hardness was very small and the hardness values approached the hardness of the base material as the depth beneath the burnished surface increased. The top layer of the burnished surface experiences work hardening process and

Table 7 – ANOVA for specific wear rate based on S/N ratio.

Parameter	Degrees of freedom	Sum of squares	Mean square	% contribution
A	2[a]	1.0576	0.5288	8.95
B	2	1.5535	0.7768	13.15
C	2	6.8259	3.4130	57.77
D	2	2.3788	1.1894	20.13
Error	0	0	–	–
Total	8	11.8158	–	100
(Error)	(2)	(1.0576)	(0.5288)	

[a] Factor A is pooled.

Table 8 – ANOVA for coefficient of friction based on S/N ratio.

Factor code	Degrees of freedom	Sum of squares	Mean square	% contribution
A	2	2.7802	1.3901	13.03
B	2	15.8211	7.9105	74.17
C	2	2.4373	1.2186	11.43
D	2[a]	0.2931	0.1466	1.37
Error	0	0	–	–
Total	8	21.3317	–	100
(Error)	(2)	(0.2931)	(0.1466)	

[a] Factor D is pooled.

Please cite this article in press as: Revankar GD, et al. Wear resistance enhancement of titanium alloy (Ti–6Al–4V) by ball burnishing process. J Mater Res Technol. 2016. http://dx.doi.org/10.1016/j.jmrt.2016.03.007

Table 10 – Optimal process parameter setting and the corresponding optimal values of specific wear rate and coefficient of friction.

Response	Optimal process parameter setting				Optimal value
	Burnishing speed (m/min)	Burnishing feed (mm/rev)	Burnishing force (N)	Number of passes	
Specific wear rate ($mm^3/N\,m$)	30	0.05	250	3	3.29×10^{-4}
Coefficient of friction	30	0.05	200	2	0.18

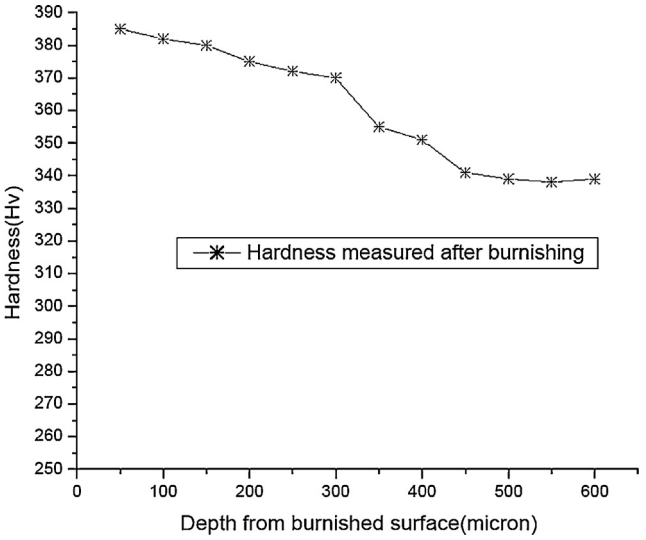

Fig. 3 – Results of surface layer microhardness tests on burnished surface for Trial No. 6 under burnishing conditions of burnishing speed – 30 m/min, feed – 0.15 mm/rev, burnishing force – 150 N and no. of passes – 2.

hence the hardness is higher than the average hardness of the work piece material.

The effect of the burnishing parameters on the surface hardness can be studied from the main effects plot in Fig. 4. From the above main effects plot in Fig. 4 on surface hardness during burnishing of titanium alloy, it is evident that surface hardness of the material increases with the increase in burnishing force and number of passes, due to work hardening and low surface hardness is observed at higher feed and speed [56–59].

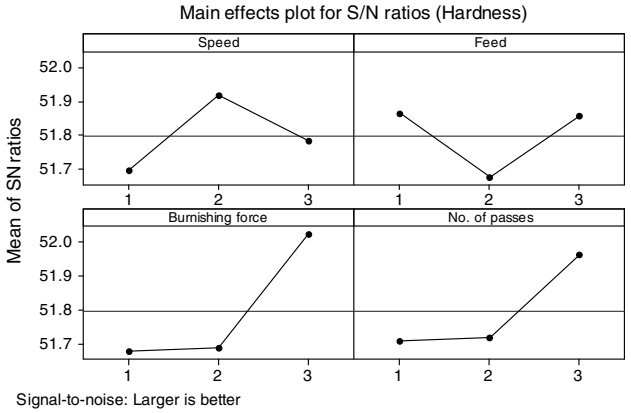

Fig. 4 – Main effects plot of hardness.

3.3. *Analysis of surface roughness*

From Table 3, it is evident that the surface roughness of the burnished surface varied in the range of 0.12–0.27 μm as compared to the turned surface whose surface roughness was 0.5 μm. In general, the obtained enhancement of surface quality (R_a) can be explained in terms of the elimination of surface irregularities that occurred by the pressing of the ball, which slides along the cylindrical surfaces with pressing burnishing force. The burnishing feed and burnishing speed have major effects in minimizing the surface roughness. Contrary, the burnishing force and number of passes have less significant role, in minimizing the surface roughness. Surface profiles of cylindrical turned and burnished surfaces (Trial No. 1) are shown in Fig. 5. The initial surface roughness after turning was R_a – 0.50 μm, whereas after burnishing for Trial No. 1 it was reduced to R_a – 0.13 μm. It can be seen that a significant decrease in surface roughness of the topography height of the work piece is obtained due to the burnishing process. Further, from Fig. 5, it is evident that burnishing had reduced surface peaks and smoothed the profile of the work piece. The image of the turned and burnished sections of the work piece is shown in Fig. 6. On the left side of the image (Fig. 6), one can clearly observe the feed marks on the turned surfaces, whereas the darker area on the right side represents a smoother burnished surface. The effect of the burnishing parameters on the surface roughness can be studied from the main effects plot in Fig. 7.

3.4. *Analysis of residual stresses*

To evaluate the degree of residual stress induced in the near surface layers by the ball burnishing, X ray diffraction measurements were performed on the turned and burnished components. It was observed that in the turned surface, tensile residual stresses are produced close to the surface, whereas after burnishing a large axial compressive macro stresses occur in the surface layer and in the near-surface regions. After analyzing the results, it was found that compression stresses occur in the surface layers of all the burnished surfaces. Fig. 8 shows the profiles of the residual stresses, as a function of depth into the surface for turned and burnished surface for Trial 3 as per experimental layout plan of our investigation (Table 2). It is obvious that after ball burnishing, compressive residual stress as high as 955 MPa was noticed immediately below the surface, and this compressive stress decays over a depth of approximately 500 μm. However, the smallest compressive stress value of 345 MPa was obtained for a workpiece Trial No. 1, subjected to a burnishing force of 150 N, speed of 15 m/min, feed of 0.05 mm/rev and one

Please cite this article in press as: Revankar GD, et al. Wear resistance enhancement of titanium alloy (Ti–6Al–4V) by ball burnishing process. J Mater Res Technol. 2016. http://dx.doi.org/10.1016/j.jmrt.2016.03.007

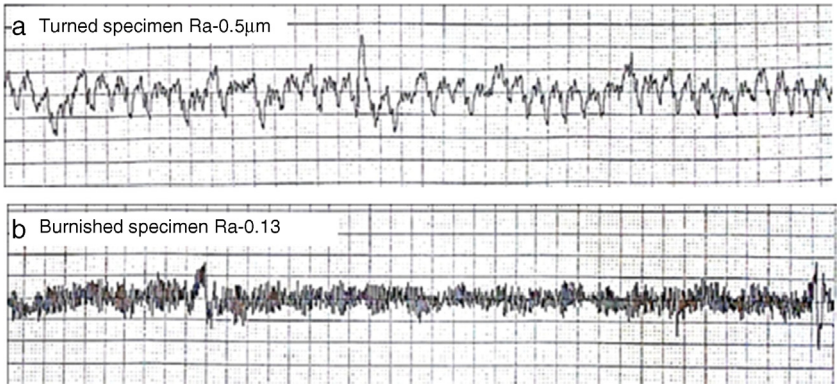

Fig. 5 – Surface profile (a) turning R_a – 0.50 μm, (b) burnishing R_a – 0.13 μm for Trial No. 1 under burnishing conditions of cutting speed – 15 m/min, feed – 0.05 mm/rev, burnishing force – 150 N and no. of passes – 1.

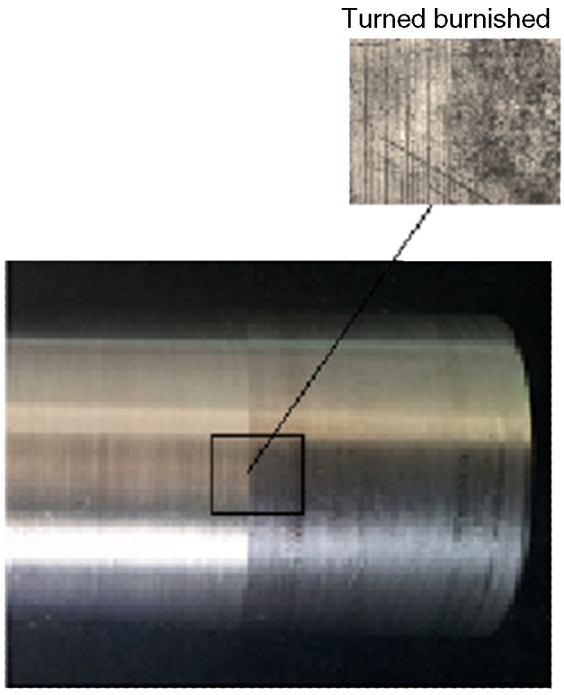

Fig. 6 – Images of turned and burnished surfaces.

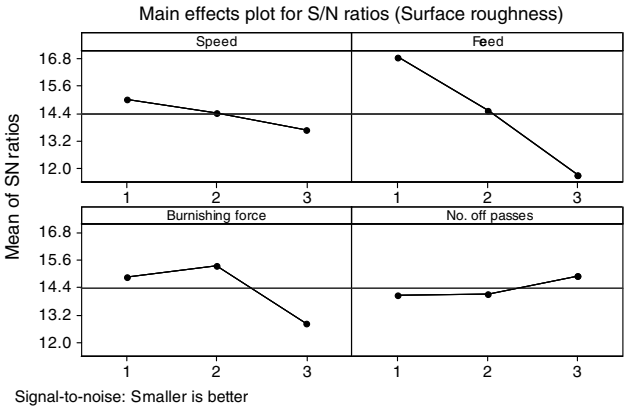

Fig. 7 – Main effects plot of surface roughness.

pass. Residual stress distribution can be affected by the burnishing parameters such as burnishing force, speed, feed and number of passes. Burnishing force has a major influence on the residual stresses. The extent of plastic deformation in the work piece enhances with the burnishing pressure and hence the magnitude of compressive residual stresses increase with increased burnishing force. The compressive residual stresses competently retard the formation and growth of cracks subjected to cyclic loading and thus enhances fatigue resistance [60,61] and vice versa for the residual tensile stresses. Hence, the residual stress on the burnished surface plays an important role, in determining the wear resistance and fatigue strength of components

3.5. *Analysis of specific wear rate*

From the ANOVA analysis in Table 7, it is evident that the strongest influence on specific wear rate was exerted by the

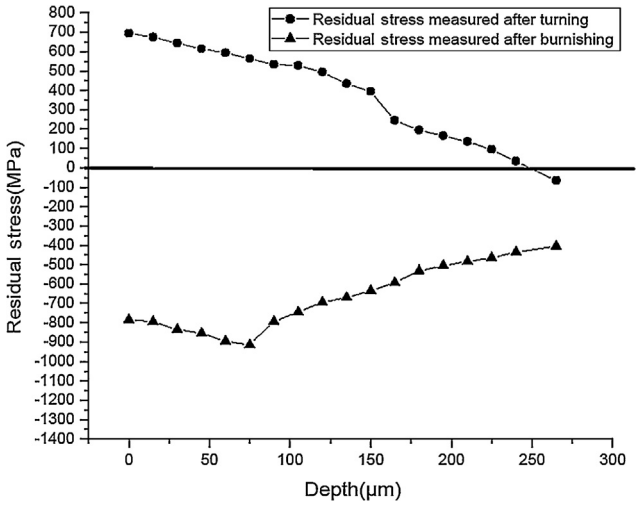

Fig. 8 – Residual stress-depth profile in Ti–6Al-4V after turning and ball burnishing. (a) Initial turned surfaces. (b) Burnishing for Trial No. 3 under burnishing conditions of burnishing speed – 15 m/min, feed – 0.15 mm/rev, burnishing force – 250 N and no. of passes – 3.

Please cite this article in press as: Revankar GD, et al. Wear resistance enhancement of titanium alloy (Ti–6Al–4V) by ball burnishing process. J Mater Res Technol. 2016. http://dx.doi.org/10.1016/j.jmrt.2016.03.007

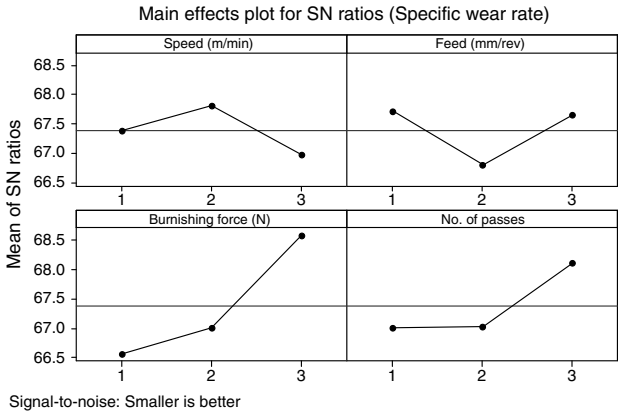

Fig. 9 – Main effects plot of specific wear rate.

burnishing force (57.77%) and number of passes (20.13%). Fig. 9 illustrates the main effects plot of burnishing parameters on specific wear rate. From Fig. 9, it is evident that the specific wear rate is reduced or an increase in wear resistance is observed with the increase in burnishing force, feed and no. of passes, whereas the specific wear rate decreases with the increase in burnishing speed. This is due to the fact that as the burnishing force increases from 150 N to 250 N, hardness of the surface is increased. The surface hardness increases rapidly with increase in burnishing force resulting in the improvement of wear resistance. Further, burnishing force increases the compressive residual stress at the surface layers, thus hindering the growth of cracks and wear delamination. On the other hand, low burnishing force leads to less improvement because the insufficient pressure results in incomplete deformation action. The variation of the specific wear rate with respect to hardness is shown in Fig. 10. The best fit line indicates a linear relationship for decrease of wear rate with hardness. Some of the results of our investigations are compared with previously published works. The study conducted by Yasuhiro et al. [62] on surface age hardening and wear

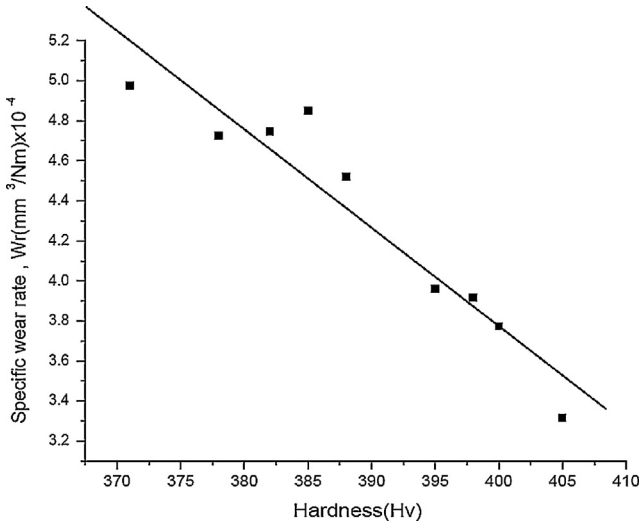

Fig. 10 – Plot showing the variation of wear rates with hardness of the burnished Ti–6Al–4V alloy.

properties of beta-type titanium alloy revealed that the wear amount of the titanium alloy decreased with the increase in hardness. Titanium has low wear and abrasion resistance because of its low hardness [63]. Because of the increase in burnishing force, the surface deformation and work hardening also increased, thus resulting in increase of surface hardness [62]. The wear resistance of titanium has been related to the sub surface deformation behavior [5,64,65]. From the experimental findings of Chan et al. [65] it has been demonstrated that wear resistance of Ti-based alloys increases with increasing hardness. It is reported in the literature that blasting of metals/metal alloys with particulate material can lead to work hardening and that this increased hardness can give rise to enhanced surface wear resistance [66]. Similar observation was reported from the studies of Rao et al. [31] that the wear resistance of HSLA Dual-Phase Steels improved with increase in burnishing force due to the plastic deformation of surface of the components by obtaining highest hardness.

The present results (Fig. 9) show that, with the increase in number of passes the specific wear rate decreases. As the no. of passes increase, the surface hardness also increases, due to condensed grain structure and increased structural homogeneity [55,56]. It can also be observed, from the main effect plot that the specific wear rate decrease with the decrease in feed. At lower feed the surface hardness is high and hence lower specific wear rate. This can be explained by the fact that, at lower feed, the plastic deformation is more rigorous causing a greater increase in surface hardness. In addition, at lower feed the number of times a ball deforms over the same spot is greater than at higher feed. The work hardening influence on the burnished surface is also greater at lower feed and decreases with increased feed. Study by El-Taweel and El-Axir [56] reveals that increase in feed, leads to decrease in surface hardness because of less work-hardening on the surface due to smaller surface area of the work piece subjected to plastic deformation.

From Fig. 9 the effects of burnishing speed on specific wear rate can be analyzed. It is observed that at low speed, the specific wear rate decreases and worsens with the rise of burnishing speed. During initial range of burnishing speed (15–30 m/min), the hardness increases, which tend to enhance the wear resistance. Because at low speed, due to more time of penetration of the burnishing tool into the burnished surface; the plastic deformation is more and hence subsequently an added amount of work hardening into the burnished surface. However, with a further increase in cutting speed in the range 30–60 m/min, the hardness decreases. This is due to the increase in recovery of the work-hardening on the surface because of the rise in temperature of the workpiece and the burnishing ball, which is associated with the increase in the rate of surface deformation as the burnishing speed increases. Moreover, at higher speed, greater frictional heat is generated as lubricant loses its effect due to limited time to interpose between the burnishing ball and work piece surface. This frictional heating promoted a temperature rise in the burnishing zone and subsequently softening of the surfaces. The increase in burnishing speed leads to instability of burnishing tool across the work piece surface and there will be incoherent deforming action of the tool, which in turn decreases hardness [31,56]. During our present study it was

Please cite this article in press as: Revankar GD, et al. Wear resistance enhancement of titanium alloy (Ti–6Al–4V) by ball burnishing process. J Mater Res Technol. 2016. http://dx.doi.org/10.1016/j.jmrt.2016.03.007

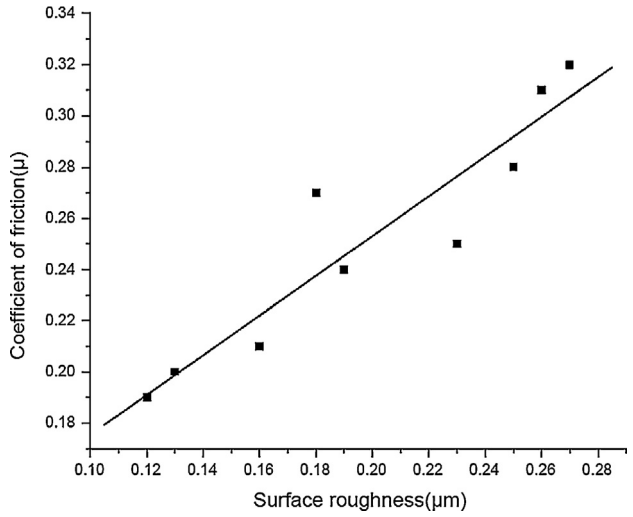

Fig. 11 – Plots showing the variation of coefficient of friction as a function of surface roughness for Ti–6Al–4V alloy subjected to burnishing.

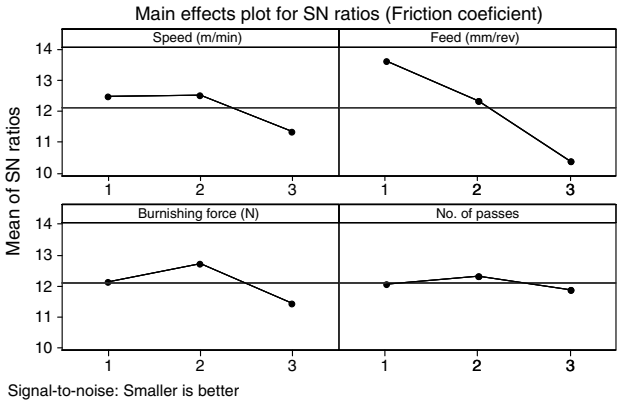

Fig. 12 – Main effects plot of coefficient of friction.

observed, higher speeds led to insufficient burnishing and probably due to which, the surface hardness might be low hence decreased wear resistance. In our study, the burnishing speed of 30 m/min was found to be suitable for improved surface hardness.

From the ANOM results as shown in Table 5, the optimal burnishing parameters for minimum specific wear rate are burnishing speed (level 2) of 30 m/min, feed (level 1) of 0.15 mm/rev, force (level 3) of 250 N and 3 no. of passes (level 3). The minimum wear rate obtained under the optimum experimental condition was 3.29×10^{-4} mm^3/N m when compared to its initial turned surface, where the corresponding value was 6.85×10^{-4} mm^3/N m. Therefore specific wear rate decreased by 52% in comparison with turned surface. The burnished surfaces in general, show better wear resistance compared to the initial turned surfaces.

3.6. *Analysis of coefficient of friction*

From the ANOVA analysis as shown in Table 6, it is evident that the strongest influence on coefficient of friction was exerted by the burnishing feed (74.17%) and burnishing speed (13.03%). The friction characteristics are evaluated in terms of coefficient of friction of the titanium alloy sliding against quenched and tempered EN-32 steel. These findings revealed that, the burnished surfaces with low surface roughness assisted in a way to reduce coefficient of friction as compared to the turned surface [33]. The coefficient of friction for the turned surface was recorded as 0.5, whereas, lowest coefficient of friction for the burnished surface under optimum condition was 0.18, which is a reduction of 64%. The variation of coefficient of friction with respect to surface roughness is shown in Fig. 11. This trend supports the fact that lower surface roughness leads to lower friction coefficient. This is because burnishing action caused the sharp and serrated tip of asperities to deform. As a result, less interlocking between the asperities led to abridge ploughing action and resulted in the decrease of friction force, whose magnitude is determined by the energy to overcome deformation.

Fig. 12 illustrates the main effects plot of burnishing parameters on coefficient of friction. It is evident from the figure that as burnishing feed increases, the coefficient of friction also increases. The coefficient of friction variation with respect to feed (Fig. 12) reveals that the at low feed, i.e., 0.05 mm/rev, the distances between the successive traces of the burnishing ball will be small, and also the ball will have more chances to smooth out the bulged edges of the previous traces as the tool passes slowly along the workpiece. This leads to a decrease in surface roughness and hence reduced coefficient of friction. At higher feed ranges, i.e., 0.10–0.25 mm/rev, the coefficient of friction drastically increases. With the progressive increase in feed, the distance between the successive burnishing ball traces increases; resulting in a reduction in likelihood for the burnishing ball to even out all the bulged edges of the former traces and therefore leading to increased surface roughness [30,56]. Also at higher feeds, the burnishing ball produces larger feed marks with a center-line distance between two succeeding indentations and hence raised surface roughness [57]. As indicated in Fig. 12, low feeds are advantageous for minimizing the surface roughness and coefficient of friction because the deforming action of the burnishing tool is greater and metal flow is regular at low feed.

From the direct plot of coefficient of friction (Fig. 12), it is observed that when the cutting speed is 15 m/min, the coefficient of friction is reduced due to reduction in surface roughness. The results revealed that less reduction in coefficient of friction was attained at lower burnishing speed 15 m/min. In the beginning, when burnishing speed is gradually increased, the work piece and burnishing ball temperature increase due to unsuitability of the burnishing tool crossing the work piece surface, consecutively increasing the material transformation between burnishing ball-work piece interfaces and hence less reduction in surface roughness [56]. With further increase in burnishing speed, from 15 m/min to 30 m/min the burnishing ball has more opportunity to settle down the abnormalities of the burnished surface and hence decreased surface roughness leading to reduced coefficient of friction. Further as the burnishing speed increases from 30 m/min to

Please cite this article in press as: Revankar GD, et al. Wear resistance enhancement of titanium alloy (Ti–6Al–4V) by ball burnishing process. J Mater Res Technol. 2016. http://dx.doi.org/10.1016/j.jmrt.2016.03.007

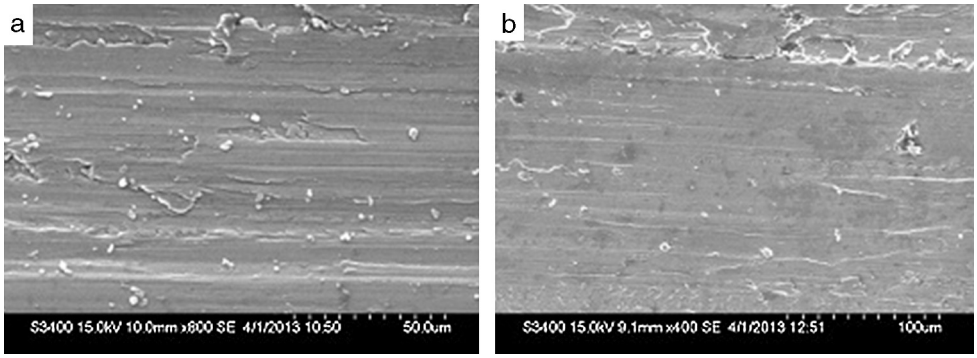

Fig. 13 – Morphology of worn surfaces of turned Ti–6Al–4V alloy sliding under different conditions under MQL conditions with a flow rate of 150 ml/h, speed of 150 m/min and a feed of 0.15 mm/rev

45 m/min, the coefficient of friction increases. The reduced lubrication effect at the burnishing zone at high speed caused a rise in temperature, leading to higher coefficient of friction. Moreover, at higher speeds mainly due to the presence of chatter and reduced amount of deformation time being offered for the burnishing tool to smooth out more irregularities, an increase in surface roughness is observed [57]. However, it can be seen that at all burnishing speed, a reduction in coefficient of friction was achieved.

As illustrated in Fig. 12, the coefficient of friction appreciably decreases for low range of forces from 150 to 200 N and the coefficient of friction increases further for higher range 200–300 N. This is due to the fact that at the commencement, the burnishing ball penetrates a little distance into a work surface, causing a little or incomplete deformation of the asperities and thus resulting into reduced coefficient of friction. When the force is slowly increased, the protrusion of work in front of the burnishing tool becomes large and the plastic deformation region broadens that in turn spoils the formerly burnished surface resulting in an enhanced surface roughness [31,57]. El-Taweel and El-Axir [56] also reported that when the burnishing ball advances further along the workpiece, the repeating plastic deformation action on the work surface leads to increased work-hardening of the earlier exaggerated layers of the deformed surface; which in turn produces flaking on the surface and hence, surface roughness increases. The diminished surface roughness noticed at higher force ranges may be probably due to increased ball pressure on work piece surface resulting in condensing the most asperities and increasing the metal flow that leads to filling of more voids and/or valleys that were exited in subsurface layer due to burnishing operation. Our experimental results closely agree with the results obtained by Lopez de et al. [67].

The surface roughness decreases when the number of passes is increased and reaches a minimum value when the number of passes is 2. However, with the further increase in the number of passes increases, the surface roughness considerably increases, thereby resulting in increase of coefficient of friction. The increase in surface roughness with more number of passes is fairly understandable because of over hardening and consequently flaking of the surface layers due to more repeated ball burnishing on work surface [56,57].

3.7. *Wear surface and wear debris*

Morphology of worn surfaces generated during wear test on turned (Fig. 13a, b) and burnished specimen of Ti–6Al–4V alloy under various burnishing conditions are shown in Fig. 14(a–f). It is evident from Figs. 13 and 14, that the worn surface of turned specimen showed signs of excessive wear as compared to that of burnished specimen. The presence of vestiges with plastic deformation and fracture was observed on the worn surfaces. Along the sliding direction the furrow and ridge were also noticed through continuous squashing and plowing by the counter face. All the wear surfaces show a typical abrasive wear. From the study of worn surfaces and sub surfaces, a tribo oxide layer was always found to form on worn surfaces and there were no traces of delaminated regions on worn surfaces. Rigney [68], confirmed by the experimental observations, that the sliding of metals can be described by the following basic wear sequence: surface and sub-surface plastic deformation, formation of debris and material transfer, reaction with the environment, mechanical mixing and producing a tribological layer. During sliding of Ti–6Al–4V alloy, tribolayer is supposed to be formed through metal debris being produced and/or transferred, ground, mixed, compacted, and even sintered on worn surfaces. In this procedure, metal debris would react with oxygen. Thus, more or less oxygen entered in tribolayer. Based on the XRD result of wear debris during wear of Ti–6Al–4V alloy, Straffelini and Molinari [8] identified two wear mechanisms for Ti–6Al–4V alloy, irrespective of the counterface and applied load, oxidation wear prevailed at the lowest sliding velocities (0.3–0.5 m/s) and delamination wear did at the highest (0.6–0.8 m/s). According to experimental study by Hsu et al. [69], plastic deformation and its accumulation on the contacting asperities control the wear process when the ambient temperature and sliding speed are not high. Subjected to a low load because of relatively higher strength of Ti–6Al–4V alloy, plastic deformation and fracture were considered to occur first on worn surface. As a result, under a low load, adhesive wear was considered to be the predominant wear mechanism, but delamination wear prevailed under a high load, where plastic deformation and fracture occurred at subsurface. Because of high hardness of steel counterface and trace tribo-oxides, the contacting asperities of counterface and oxidized wear debris would plow the surface of

Please cite this article in press as: Revankar GD, et al. Wear resistance enhancement of titanium alloy (Ti–6Al–4V) by ball burnishing process. J Mater Res Technol. 2016. http://dx.doi.org/10.1016/j.jmrt.2016.03.007

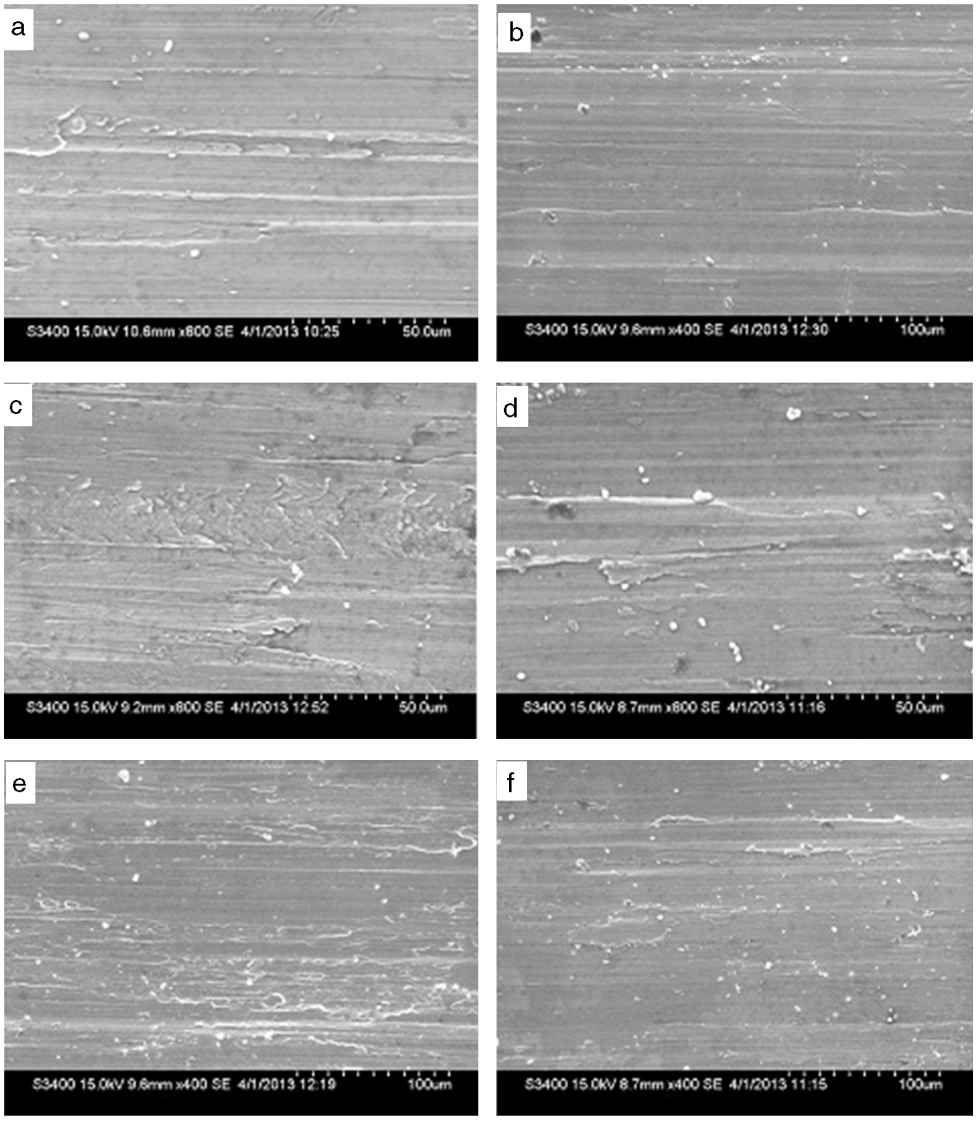

Fig. 14 – Morphology of worn surfaces of burnished Ti–6Al–4 V alloy sliding under different conditions. (a) At $v = 30$ m/min, $f = 0.05$ mm/rev, $F = 200$ N, $n = 3$. (b) At $v = 30$ m/min, $f = 0.10$ mm/rev, $F = 250$ N, $n = 1$. (c) At $v = 45$ m/min, $f = 0.10$ mm/rev, $F = 150$ N, $n = 3$. (d) At $v = 15$ m/min, $f = 0.10$ mm/rev, $F = 200$ N, $n = 2$. (e) At $v = 15$ m/min, $f = 0.15$ mm/rev, $F = 250$ N, $n = 3$. (f) At $v = 15$ m/min, $f = 0.05$ mm/rev, $F = 150$ N, $n = 1$.

Ti–6Al–4Valloy, producing furrow and ridges on worn surfaces. Hence, it is suggested that adhesive wear and delamination wear prevailed at 25–200 °C, accompanying abrasive wear. Under the experimental conditions, even though the sliding speed is high at 2.68 m/s, delamination wear was not observed contrary to the views of Straffelini and Molinari [8]. However, since the load is low at 10 N there was no delamination wear, consistent with the work of Hsu et al. [69]. Wear debris can act as a very useful diagnostic tool for finding out the mechanism of wear. In our work, the wear debris, obtained was in the form of a powder, unlike flake-like metallic wear particles, which indicate that delamination occurs during wear [70]. Titanium alloy commonly transfers to the counterface when rubbing against other metals or ceramics [2,7,10]. The steel counterpart surfaces typically exhibited minor micro-plowing wear scars aligned parallel to the reciprocating-sliding direction together with a high density of heavily flattened patches and smeared metal prows aligned in the sliding direction. Energy dispersive X-ray analysis of the worn surfaces showed that transfer of the steel counterpart to the titanium pins had occurred during wear mechanism.

3.8. *EBSD analysis*

Electron backscattered diffraction (EBSD) observation in the present study was performed at a depth of 100 μm from the top surface owing to the ultrafine grains in the top surface of burnished samples. The orientation EBSD images of the titanium alloy before and after deformation are shown in Fig. 15. As shown in Fig. 15, the color of the grains indicates the different orientation and the similar color means the grains have the similar orientation. Fig. 15(a) shows the image before

Please cite this article in press as: Revankar GD, et al. Wear resistance enhancement of titanium alloy (Ti–6Al–4V) by ball burnishing process. J Mater Res Technol. 2016. http://dx.doi.org/10.1016/j.jmrt.2016.03.007

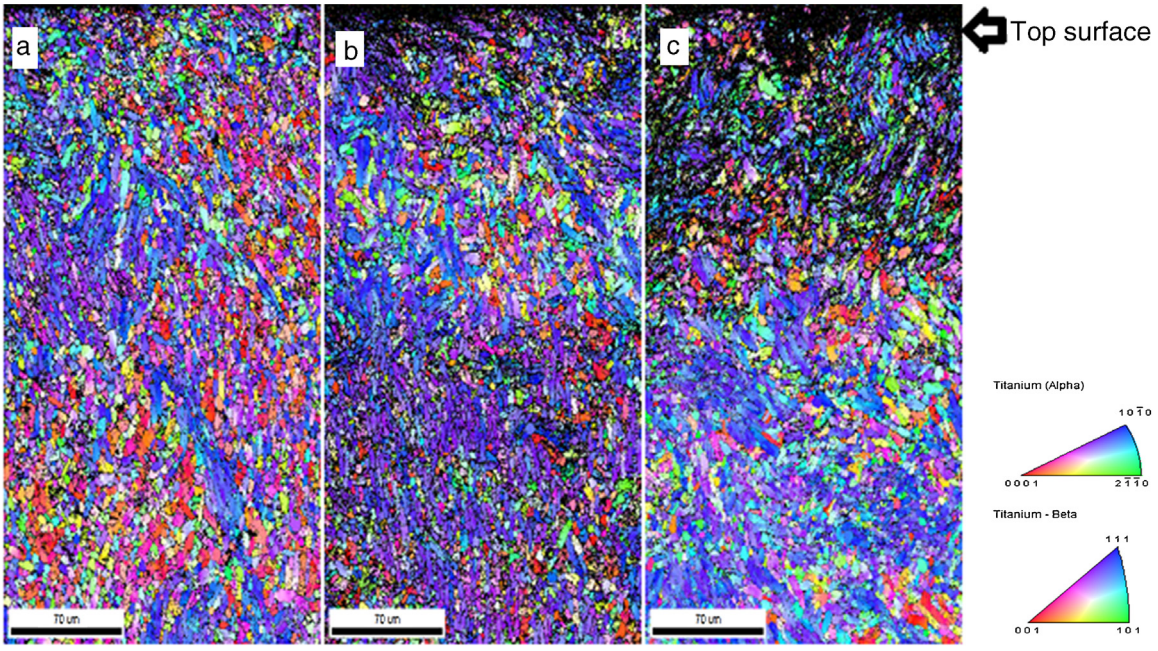

Fig. 15 – EBSD image morphology of turned and burnished surfaces Ti–6Al–4 V alloy specimens. (a) Turned specimen MQL conditions with a flow rate of 150 ml/h, speed of 175 m/min and a feed of 0.05 mm/rev. (b) Burnished at $v = 15$ m/min, $f = 0.10$ mm/rev, $F = 200$ N, $n = 2$. (c) Burnished at $v = 15$ m/min, $f = 0.15$ mm/rev, $F = 250$ N, $n = 3$.

deformation, i.e., after turning. Some grains were elongated in the specimen deformed as shown in Fig. 15(b), when further deformed by increasing the burnishing force, dislocations can be observed as shown in Fig. 15(c). EBSD observations reveal that the density of sub-grain boundaries and high angle grain boundaries increased during deformation, clearly indicating that dislocation sliding and climbing are important processes during deformation [71]. The experiment results indicate the superplastic deformation is controlled by grain boundary sliding and dislocation motion.

3.9. *Microstructural analysis*

The cross-sectional microstructures, near the topmost surface regions, of turned and burnished surfaces under different burnishing conditions are shown in Fig. 16. The direction of arrow in these figures indicates the top surface. The turned surface displays no change in the grain size near the surface. However, due to burnishing process, owing to the driving of the burnishing force and friction force introduced between specimens and burnishing tool, the grains become sheared and grain size decreases dramatically. It is evident from these figures that adjacent to the burnished surface, a layer existed where the grain boundaries were not discernable under the current observation method. This featureless layer has no identifiable grain structure and indiscernible grain boundaries were also reported in Ti–6Al–4V after deep rolling [60]. The layer influenced by burnishing is described as a layer where the microstructure exhibits the features of recrystallized grains, elongated sub grains, and/or grains with heavy twinnings and stacking-faults [72]. A different microstructure is observed after deformation due to burnishing, no nanocrystallites were formed, but the dislocation arrangement consisted of diffuse tangled and debris-like structures, cell formation was not observed, and the dislocation arrangement was almost entirely planar [73]. This result indicates that the increase in the deformation promotes the generation of dynamic recrystallization, which results from the significant near-surface increase in dislocation density and lattice distortion. After this layer, as observed from the figures, the bulk microstructure appears, which is considered as the end of burnishing influenced layer.

3.10. *Residual stresses estimation using a FEM model*

An attempt has been made to present a FE model for ball burnishing. Here, the geometry and the mesh were created using LS-PrePost. This is an advanced pre and post-processor tool from Livermore Software technology corporation (LSTC). Due to large variation in the stress components throughout the layers beneath the contact zone, small elements should be assigned to this region. From the study conducted by Liu Y et al. [74], it is revealed that proportion of the smallest size to the diameter of dimple generated in the contact zone is recommended to be about 1/10th in the ball burnishing process. The geometric workpiece model considered in the 3D FEM simulations is shown in Fig. 17. The workpiece is modeled by a portion of a cylindrical part. The choice of workpiece size in 3D FEM simulations takes into account the real dimensions of the treated piece, the presented boundary conditions and the optimization of computational time. The external radius is equal to the rod bar radius, which is utilized in experimental work. The mesh generated of the ball tool and the workpiece in the 3D ball burnishing simulation are shown in Fig. 17.

Please cite this article in press as: Revankar GD, et al. Wear resistance enhancement of titanium alloy (Ti–6Al–4V) by ball burnishing process. J Mater Res Technol. 2016. http://dx.doi.org/10.1016/j.jmrt.2016.03.007

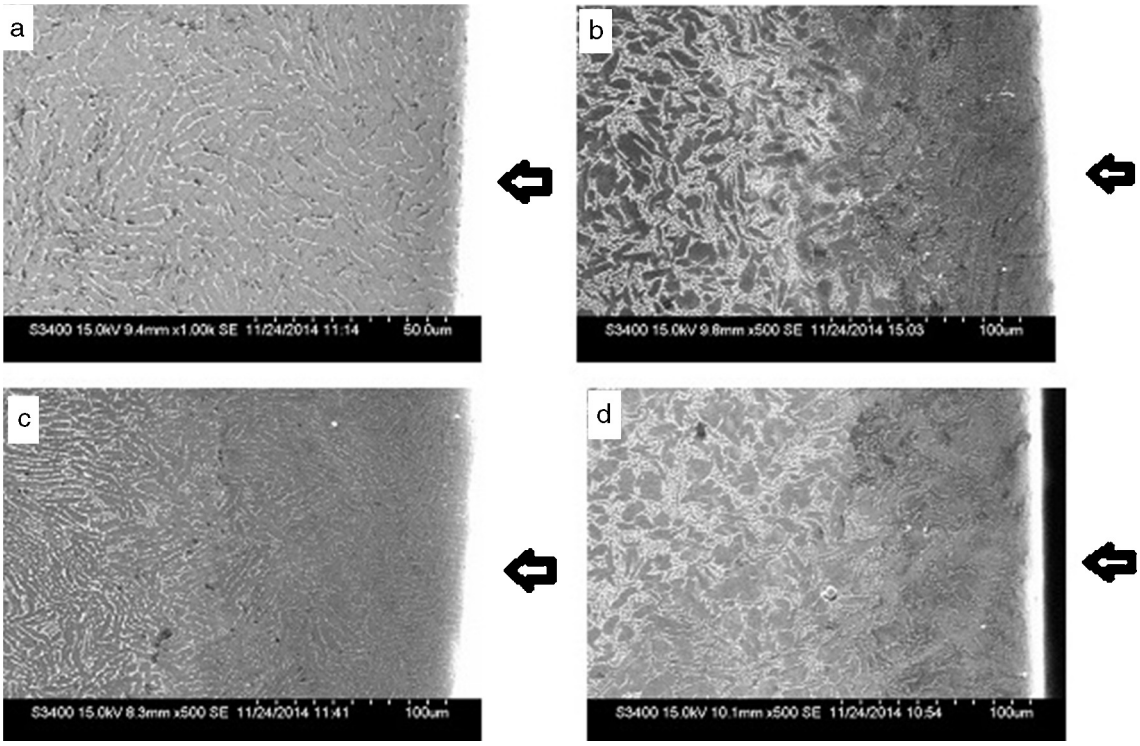

Fig. 16 – SEM images of the cross section at the topmost surfaces under different burnishing conditions. (a) Burnished at $v = 30$ m/min, $f = 0.05$ mm/rev, $F = 200$ N, $n = 3$. (b) Burnished at $v = 15$ m/min, $f = 0.10$ mm/rev, $F = 200$ N, $n = 2$. (c) Burnished at $v = 15$ m/min, $f = 0.15$ mm/rev, $F = 250$ N, $n = 3$. (d) Burnished at $v = 45$ m/min, $f = 0.15$ mm/rev, $F = 200$ N, $n = 1$ (direction of arrow indicates the top surface).

As described, in the contact zone, fine elements should be used. However, in the regions, which are far away from the contact zone, course elements can be generated to decrease the number of degrees of freedom and computational costs. Smooth transition between the fine and coarse elements should be provided using intermediate elements. In this study, linear tetrahedral elements are used to discretize the work piece and ball. Taking these facts into consideration the mesh for the specimen was created such that at the area of contact the element size was very fine and gradually the mesh was coarsened out. This helped to minimize the number of element count. FEM analysis was carried out with sufficient mesh density in the region of burnishing and lesser density elsewhere. Initially, to determine the effect of the mesh density on computational accuracy, processing time and program convergence, different types of FE mesh were prepared and studied for the 3D model. Finally, a FE model with 283,550 eight-node C3D8R elements and 300,456 nodes was prepared with increased mesh density in the area close to the surface, as shown in Fig. 18. Rotating quads were used in order to achieve transition of mesh. Solid brick element having Elform 2 (fully integrated elements) were used. The spherical indenter was modeled with rigid shell elements having properties of tungsten carbide material and the Ti–6Al–4V workpiece was modeled considering as kinematic plastic material.

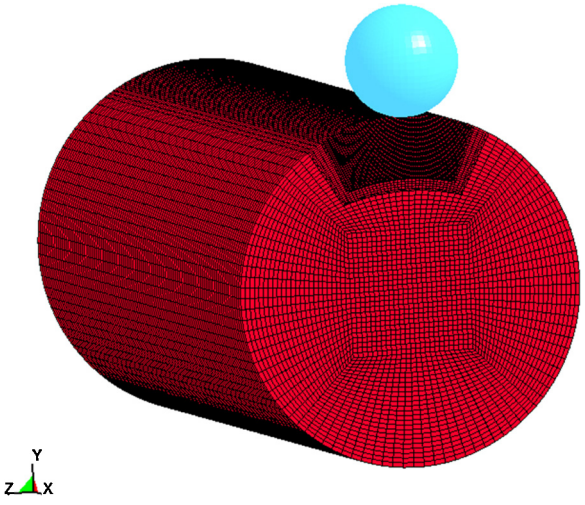

Fig. 17 – Meshing of the ball tool and the workpiece in the 3D ball burnishing simulation.

The FE model is based on the following assumptions:

1. The ball tool is considered rigid and is modeled by an analytically rigid part.
2. The work piece is considered as kinematic plastic material.
3. The surface roughness profile is neglected.
4. The ball burnishing speed effect is neglected.

The Johnson–Cook model has been widely used in the literatures to characterize Ti–6Al–4V. In this model, the material properties not only depend on the strain, but also depend on the temperature and strain rate. Johnson–Cook constitutive

Please cite this article in press as: Revankar GD, et al. Wear resistance enhancement of titanium alloy (Ti–6Al–4V) by ball burnishing process. J Mater Res Technol. 2016. http://dx.doi.org/10.1016/j.jmrt.2016.03.007

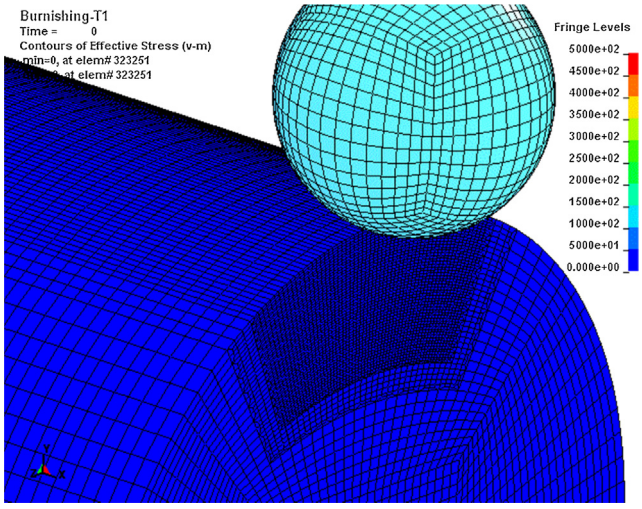

Fig. 18 – Discretization of the ball and the workpiece in the 3D ball burnishing simulation.

model for Ti–6Al–4V is a simple numerical material model developed for isotropic material. In this material model, it is assumed that elastic strains are negligible in comparison to plastic strain. The elastic domain is defined by means of the Von-Mises yield criterion, and it is assumed that isotropic strain hardening is sufficient to describe the evaluation of the yield surface during plastic deformation. Strain hardening is thus described in terms of the damage accumulated plastic strain. It is further assumed that the elastic and visco-plastic properties of the material depend on the temperature generated by adiabatic heating under high strain rate loading conditions, while any thermo-mechanical coupling with the surrounding is not included in the formulation. The movement of the ball with respect to workpiece can be controlled by the displacement of tool. This method would require information on the ball penetration depth for the given process settings. This depth value, involving plastic deformation, changes from one cycle to another. It cannot be solved analytically due to the nonlinearity of the workpiece properties and is usually very difficult to measure during ball burnishing experiments. The relationship between the force and ball penetration depth is obtained from series ball burnishing simulations. To apply the required burnishing force during simulation, the corresponding penetration depth is calculated from a 3D indentation simulation test results. The movement of the ball in the simulation can be controlled, by using two different ball movement controls, that is, displacement control and force control. In the force control, the ball presses on the work piece until the maximum applied load is reached for every indentation cycle. This type of loading does not strictly reflect the real load applied to the part during cylindrical rolling. Indeed, the real contact is a sphere/cylinder one, whereas the 2D model simulates a cylinder/plane contact.

For these reasons, it is preferred to use the displacement control method in the 3D FEM. This load is a succession of three repetitive movements. To attain a sufficient simulation area, eight cycles of the burnishing process were carried out. The load stages of each cycle are given below:

Stage 1: the ball traverses down vertically applying the corresponding burnishing force related to the phase of penetration into the material (loading)
Stage 2: the ball traverses to the initial position (unloading)
Stage 3: the ball traverses horizontally with a displacement value of burnishing feed (feed per revolution)

The specimen was fixed axially at one end in translation DOF. To reduce the analysis time, it was assumed that the same effect of experiment would be achieved if the specimen was not rotated and if the indenter moved axially on the surface of specimen. Nodes to surface contact were evoked in order to get a better correlation of the results. Considering the fact that sliding between analytical rigid ball and deformable workpiece is inevitable, the simulation has been conducted so that the friction has been introduced in order to avoid sliding between the ball and workpiece as assumed in the study given by Fischer-Cripps [75]. A friction parameter of $\mu = 0.3$, was assumed for the contact between the tool and the workpiece during modeling as per the classical Coulomb law. The spring-back analysis was conducted after ball burnishing, in order to achieve the steady state of residual stress profile. However, it was found that this analysis was not practical to be simulated, since long time is required to reach the steady state. Thus implicit method was used to simulate the spring-back analysis, since after removing the ball there is no complexity due to contact between the parts and consequently different nonlinearities are not involved in the spring- back problem. In conducting the simulations, the following burnishing conditions were used:

- Burnishing ball diameter = 8 mm
- Burnishing force (N) = 150, 200, 250, 300 and 350
- Burnishing feed rate (mm/rev) = 0.05, 0.10, 0.15, 0.20 and 0.25
- Number of passes = 1

3.10.1. *Effect of burnishing feed on residual stress*

To study the distribution of the residual stresses using different values of burnishing feed ($f = 0.05$, 0.10, 0.15, 0.20 and 0.25 mm/rev) with a burnishing force of 200 N, FEM simulations were carried out. Fig. 19 shows the effect of burnishing feed on the experimental and simulated residual stress distribution. It is evident from Fig. 19 that the predicted values of axial and tangential residual stress, under different feed rate are in good agreement with the experimental values. The effect of feed rate on residual stress is consistent with experimental observations. From the FEM simulation results in Fig. 19, it is clear that a decrease in the burnishing feed slightly raises the magnitude of the compressive residual stresses in both axial and tangential directions. This can be explained by the fact that a small feed indicates shorter distance between ball traces. As a result, the workpiece surface was subjected to greater amount of plastic deformation and residual stresses due to more repetitive compression by the ball tool. Simulations showed greater influence of burnishing feed rate on tangential residual stresses i.e., more variation of residual stresses in tangential direction due to change in burnishing feed. However it was found that the magnitudes of the residual stresses are weak, for different values of feed. Thus, it can be concluded

Please cite this article in press as: Revankar GD, et al. Wear resistance enhancement of titanium alloy (Ti–6Al–4V) by ball burnishing process. J Mater Res Technol. 2016. http://dx.doi.org/10.1016/j.jmrt.2016.03.007

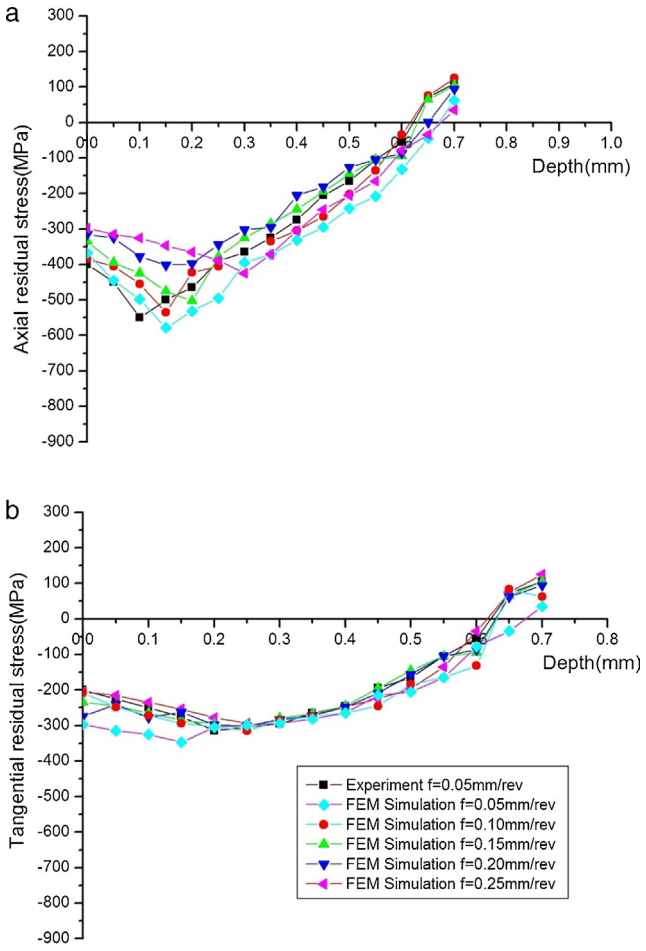

Fig. 19 – Simulation of the axial (a) and tangential (b) residual stress state after burnishing using different burnishing feed (f = 0.05, 0.10, 0.15, 0.20 and 0.25 mm/rev) and F = 200 N.

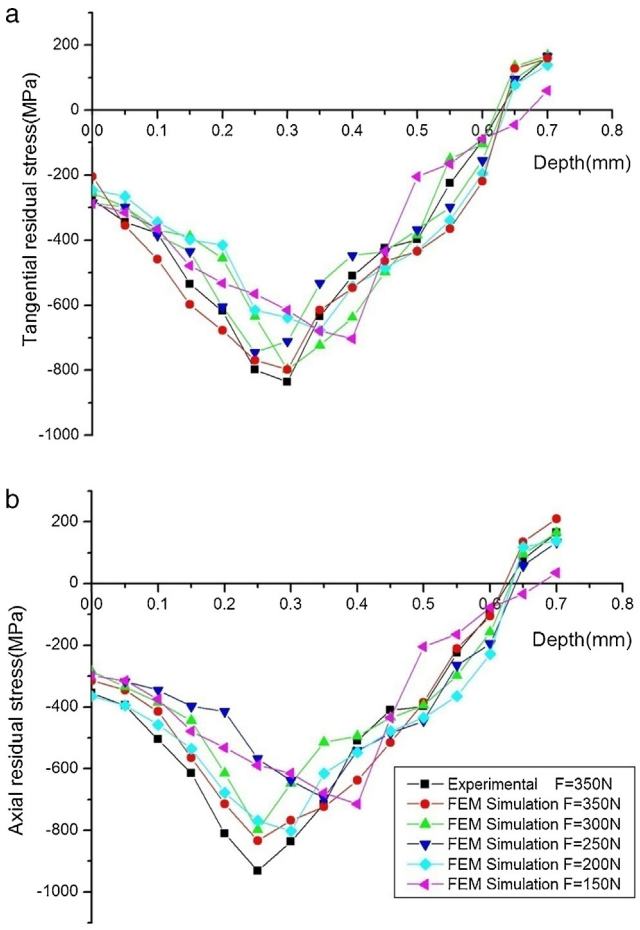

Fig. 20 – Simulation of the axial (a) and tangential (b) residual stress state after burnishing using different burnishing force (F = 150, 200, 250, 300, 350 N) and burnishing feed (f = 0.05 mm/rev).

from FEM simulations that the axial and the tangential residual stresses are not significantly influenced by the feed [48].

3.10.2. *Effect of burnishing force on residual stress*

To study the distribution of the residual stress under different burnishing pressures (F = 150, 200, 250, 300 and 350 N) with a burnishing feed rate of 0.05 mm/rev, various FEM simulations were carried out. Fig. 20 shows the effect of burnishing pressure on the experimental and simulated residual stress distribution. Because of burnishing, compressive residual stresses were obtained in both axial and tangential direction. It was also evident that with the increase in burnishing pressure, higher residual stresses were generated at a greater depth. It is evident from Fig. 20 that the predicted values of axial and tangential residual stress, under different values of burnishing force with a feed rate of 0.05 mm/rev are in good agreement with the experimental values. The residual stress gradually increases up to a certain depth from the surface and achieves maximum value in the sub-surface and then decreases as we go deep into the surface. As Fig. 20 indicates, both FEA and experimental results show similar variations with respect to depth. To further study the effect of burnishing force on residual stress, different simulations were tried out under different magnitudes of burnishing force, keeping the feed rate constant. The results qualitatively agree with the experimental results. Higher burnishing pressures generate more compressive residual stress near the surface and produce a deeper effective compressive stress layer. The occurrences of maximum residual compressive stress, its magnitude and depth at which it occurs follow similar trend in both techniques. The induced residual compressive stress values obtained from FEA are compared with the experimental X-ray diffraction results and the deviation is found to be less than 16%. As the burnishing force increases the compressive residual stresses also increase. The increase of applied burnishing force leads to an increase in the amount of plastic deformation as more roughness valleys are filled, during the process. It is established from Fig. 20 that the depth and maximum values of the residual stresses considerably increases with the increase in burnishing force. These results also agree with experimental study by Farough [76] during low plasticity burnishing process of titanium alloy. From the present study, it is evident that, with the increase in penetration depth, an increase in the burnishing force applied to the surface is observed, which leads to increase in the surface hardness and

Please cite this article in press as: Revankar GD, et al. Wear resistance enhancement of titanium alloy (Ti–6Al–4V) by ball burnishing process. J Mater Res Technol. 2016. http://dx.doi.org/10.1016/j.jmrt.2016.03.007

compressive residual stresses [59]. These results are qualitatively in agreement with the results of Sartkulvanich et al. [47], Bougharriou et al. [48] and Sayahi et al. [77]. Therefore, it can be concluded from the results that, if the only objective of surface treatment is to generate high residual stresses, the best choice is to burnish with the maximum pressure. But, increasing the burnishing pressure can result in increase of surface roughness and geometrical error, which has to be monitored.

4. Conclusions

The results obtained from the surface quality and tribology studies indicates that ball burnishing process has good prospects to be introduced as a new surface treatment method for titanium alloy. Based on the analysis of the experimental results, the following conclusions can be drawn from the present investigation.

- After burnishing, surface microhardness increased from 340 to 405 HV, whereas surface roughness decreased from 0.45 to 0.12 μm and compressive residual stress, as high as 955 MPa, was noticed immediately below the surface.
- A combination of burnishing speed in the medium range, low feed, high burnishing force with three passes is helpful to minimize specific wear rate. However, burnishing with medium speed, low feed, medium force and two numbers of passes could minimize the coefficient of friction.
- It is evident that the specific wear rate is reduced with the increase in burnishing force, feed and no. of passes, however specific wear rate decreases with the increase in burnishing speed.
- It is observed that the coefficient of friction decreases with the increase in burnishing feed, speed and number of passes, however, it increases with the increase in burnishing force.
- The burnishing force and number of passes with contribution of 57.77% and 20.13% have major effects in minimizing the specific wear rate. Contrary, the burnishing feed and burnishing speed with contribution of 74.17% and 13.03% have key roles in minimizing the coefficient of friction.
- Taguchi optimization in this investigation, showed greater improvements in specific wear rate 3.29×10^{-4} mm^3/N m (52% decrease) and coefficient of friction 0.18 (64% decrease), when compared to turned surfaces.
- Predictions of residual stress distributions beneath the burnished surfaces with the developed 3D FEM model are in good agreement with the experimental measurements obtained using X-ray diffractions.
- The surface quality and tribological characteristics of titanium alloy Ti–6Al–4V can be improved by ball burnishing, showing improved friction and wear performance.

Burnishing process is an emerging, hot topic in the manufacturing field and the benefits of this process are vast. Hence, further works can be extended related with the improvement in fatigue performance of burnished components, with the models for burnishing and to study the evolution mechanisms of the ultrafine grain and texture in the burnished surface layer.

Conflicts of interest

The authors declare no conflicts of interest

Acknowledgement

The authors would like to thank SAIF, IIT Bombay, India for providing facilities to carry out the EBSD analysis.

REFERENCES

[1] Chunxiang C, BaoMin H, Lichen Z, Shuangjin L. Titanium alloy production technology, market prospects and industry development. Mater Des 2011;32:1684–91.
[2] Budinski KG. Tribological properties of titanium alloys. Wear 1991;151:203–17.
[3] Yerramareddy S, Bahadur S. The effect of laser surface treatments on the tribological behavior of Ti–6Al–4V. Wear 1992;157:245–62.
[4] Grenier M, Dubé D, Adnot A, Fiset M. Microstructure and wear resistance of CP titanium laser alloyed with a mixture of reactive gases. Wear 1997;210:127–35.
[5] Long M, Rack H. Titanium alloys in total joint replacement—a materials science perspective. Biomaterials 1998;19:1621–39.
[6] Agins HJ, Alcock NW, Bansal M, Salvati E, Wilson PO, Pellicci PM, et al. Metallic wear in failed titanium-alloy hip replacements. J Bone Joint Surg Am 1988;170A(3):347–56.
[7] Molinari A, Straffelini G, Tesi B, Baccai T. Dry sliding wear mechanism of the Ti6Al4V alloy. Wear 1997;208:105–12.
[8] Straffelini G, Molinari A. Dry sliding wear of Ti–6Al–4Valloy as influenced by the counterface and sliding conditions. Wear 1999;236:328–38.
[9] Alam Ohidul MD, Haseeb ASMA. Response of Ti–6Al–4V and Ti–24Al–11Nb alloys to dry sliding wear against hardened steel. Tribol Int 2002;35:357–62.
[10] Dong H, Bell T. Tribological behaviour of aluminium sliding against Ti6Al4V in unlubricated contact. Wear 1999;225–229:874–84.
[11] Qiu M, Zhang YZ, Zhang JH, Zhu J. Microstructure and tribological characteristics of Ti–6Al–4V alloy against GCr15 under high speed and dry sliding. Mater Sci Eng 2006;434A:71–5.
[12] Magaziner RS, Jain VK, Mal S. Investigation into wear of Ti–6Al–4V under reciprocating sliding condition. Wear 2009;267:368–73.
[13] Manisavagam G, Amritpreet KS, Rajamanickam A, Ashok KG. Ti based biomaterials: the ultimate choice for orthopaedic implants – a review. Prog Mater Sci 2009;54(3):397–425.
[14] Johnson R, Eberhardt J. Thermal oxidation: a promising surface treatment for titanium engine parts. Transportation Program Oak Ridge National Laboratory; 2006.
[15] Xuanyong L, Paul KC, Chuanxian D. Surface modification of titanium, titanium alloys and related materials for biomedical application. Mater Sci Eng R 2004;47:49–121.
[16] Guleryuz H, Cimenoglu H. Surface modification of a Ti–6Al–4V alloy by thermal oxidation. Surf Coat Technol 2005;192:164–70.
[17] Borgioli F, Galvanetto TE, Lozzelli F, Pradelli G. Improvement of wear resistance of Ti–6Al–4V alloy by means of thermal oxidation. Mater Lett 2005;59:2159–62.
[18] Morton PH, Bell T. Surface engineering of titanium. Mémoires et Ëtudes Scientifiques Revue de Métallurgie 1989;86(10):639–46.

Please cite this article in press as: Revankar GD, et al. Wear resistance enhancement of titanium alloy (Ti–6Al–4V) by ball burnishing process. J Mater Res Technol. 2016. http://dx.doi.org/10.1016/j.jmrt.2016.03.007

[19] Chengwei C, Zhiming Z, Xitang T, Wang Y, Sun XT. Influence of rapidly solidified structures on wear behavior of Ti–6Al–4V laser alloyed with TiC. Tribol Trans 1995;38(4):875–8.
[20] Streicher RM, Weber H, Schon R, Semlitsch M. New surface modification for Ti–6Al–7Nb alloy: oxygen diffusion hardening (ODH). Biomater 1991;12:125–9.
[21] Zwicker J, Etzold U, Moser TH. Abrasive properties of oxide layers on Ti–Al15–Fe2.5 in contact with high density polyethylene. In: Lütjering G, Zwicker U, Bunk W, editors. Titanium'84 Science and Technology, vol. 2. 1985. p. 1343–50 (Proc. of the 5. Int. Conf. on Titanium, Munich).
[22] Mishra SC, Nayak BB, Mohanty BC, Mills B. Surface nitriding of titanium in arc plasma. J Mater Process Technol 2003;132:143–8.
[23] Luo Y, Ge S, Liu H, Jin Z. Microstructure analysis and wear behavior of titanium cermet femoral head with hard TiC layer. J Biomech 2009;42:2708–11.
[24] Kartal G, Timur S, Urgen M, Erdemir A. Electrochemical boriding of titanium for improved mechanical properties. Surf Coat Technol 2010;204:3935–9.
[25] Alves C Jr, Guerra Neto C, Morais G, Silva C, da Hajek V. Nitriding of titanium disks and industrial dental implants using hollow cathode discharge. Surf Coat Technol 2005;194:196–202.
[26] David F, Liam N, Greg B, Nicholas B, Denis PD. Wear resistance enhancement of the titanium alloy Ti–6Al–4V via a novel co-incident micro blasting process. Surf Coat Technol 2011;205:4941–7.
[27] Ganesh BKC, Sha W, Ramanaiah N, Krishnaiah A. An effect of shot peening on sliding wear and tensile behavior of titanium implant alloys. Mater Des 2014;56:480–6.
[28] El-Tayeb NSM. Frictional behaviour of burnished copper surfaces under dry contact conditions. HU, Cairo: Engineering Research Bulletin; 1994. p. 171–84.
[29] El-Tayeb NSM, Ghobrial MI. The mechanical wear behaviour of burnishing surfaces. In: Proc. 4th international conference on production engineering and design for development. 1993. p. 198–209.
[30] El-Tayeb NSM, Low KO, Brevern PV. Enhancement of surface quality and tribological properties using ball burnishing process. Mach Sci Technol 2008;12:234–48.
[31] Rao DS, Suresh HH, Komaraiah M, Kempaiah UN. Investigations on the effect of ball burnishing parameters on surface hardness and wear resistance of HSLA dual-phase steels. Mater Manuf Process 2008;23:295–302.
[32] Rajasekariah R, Vaidyanathan S. Increasing the wear-resistance of steel components by ball burnishing. Wear 1975;34:183–8.
[33] Low KO, Wong KJ. Influence of ball burnishing on surface quality and tribological characteristics of polymers under dry sliding conditions. Tribol Int 2011;44:144–53.
[34] Luca LL, Neagu SV, Marinescu I. Effects of working parameters on surface finish in ball-burnishing of hardened steels. Prec Eng 2005;29:253–6.
[35] Korzynski M. Modeling and experimental validation of the force-surface roughness relation for smoothing burnishing with a spherical tool. Int J Mac Tools Manuf 2007;47:1956–64.
[36] Feng LL, Wei X, Zhao YZ, Jing Z, Zheng QT. Analytical prediction and experimental verification of surface roughness during the burnishing process. Int J Mac Tools Manuf 2012;62:67–75.
[37] Radoslaw WM, Stanislaw L, Grzegorz MK, Pero R. Influence of cooling conditions on the machining process under MQCL and MQL conditions. Tehnicki Vjesnik Technical Gazette 2015;22(4):965–70.
[38] Radoslaw WM, Krolczyk GM, Feldshtein E, Szydlowski M, Legutko S, Pusavec F, et al. A study on droplets sizes, their distribution and heat exchange for minimum quantity cooling lubrication (MQCL). Int J Mach Tools Manuf 2016;100:81–92.
[39] Krolczyk G, Nieslony P, Legutko S, Microhardness. Surface Integrity in turning process of duplex stainless steel (DSS) for different cutting conditions. J Mater Eng Perform 2014;23(3):859–66.
[40] Bouzid W, Tsoumarev O, Sai K. An investigation of surface roughness of burnished AISI 1042 steel. Int J Adv Manuf Technol 2004;24(1–2):120–5.
[41] Mieczyslaw K. Modeling and experimental validation of the force–surface roughness relation for smoothing burnishing with a spherical tool. Int J Mach Tools Manuf 2007;47:1956–64.
[42] El-Axir MH, Othman OH, Abodiena AM. Study on the inner surface finishing of aluminum alloy 2014 by ball burnishing process. J Mater Process Technol 2008;202:435–42.
[43] Skalski K, Morawski A, Przybylski W. Analysis of contact elastic–plastic strains during the process of burnishing. Int J Mech Sci 1995;37(5):461–72.
[44] Röttger K [PhD dissertation] Walzen hartgedrehter Oberflaechen. Technical University of Aachen; 2002.
[45] Beres W, Li J, Patnaik PC. Numerical simulation of the low plasticity burnishing process for fatigue property enhancement. ASME Turbo Expo 2004: Power Land Sea Air 2004;4:809–18.
[46] Bouzid W, Sai K. Finite element modeling of burnishing of AISI 1042 steel. Int J Adv Manuf Technol 2005;25:460–5.
[47] Sartkulvanich P, Altan T, Jasso F, Rodriguez C. Finite element modelling of hard roller burnishing: an analysis on the effects of process parameters upon surface finish and residual stress. J Manuf Sci Eng Trans ASME 2007;129:705–16.
[48] Bougharriou A, Sai WB, Sai K. Prediction of surface characteristics obtained by burnishing. Int J Adv Manuf Technol 2010;51(1–4):205–15.
[49] Maximov JT, Duncheva GV. Finite element analysis and optimization of spherical motion burnishing of low-alloy steel. Proc I Mech E C J Mech Eng Sci 2011;226:161–76.
[50] Revankar GD, Shetty R, Shrikantha SR, Gaitonde VN. Analysis of surface roughness and hardness in titanium alloy machining with polycrystalline diamond tool under different lubricating modes. Mater Res 2014;17(4):1010–22.
[51] Revankar GD, Shetty R, Shrikantha SR, Gaitonde VN. Selection of optimal process parameters in ball burnishing of titanium alloy. Mach Sci Technol Int J 2014;18(3):464–83.
[52] Phadke MS. Quality engineering using robust design. Englewood Cliffs, NJ: Prentice-Hall International, Inc; 1989.
[53] Ross PJ. Taguchi techniques for quality engineering. 2 ed. New York: McGraw-Hill; 1996.
[54] ASTM. Designation G99-95; standard test method for wear testing with a pin-on-disk apparatus; 1995. p. 336–90.
[55] Bressan JD, Hesse R. Construction and validation tests of pin-on-disc equipment. In: XVI Congresso Brasileiro de Engenharia Mecânica, COBEM 2001. 2001.
[56] El-Taweel TA, El-Axir MH. Analysis and optimization of the ball burnishing process through the Taguchi technique. Int J Adv Manuf Technol 2009;41:301–10.
[57] Hassan AM, Al-Jalil HF, Ebied AA. Burnishing force and number of tool passes for the optimum surface finish of brass components. J Mater Process Technol 1998;83:176–9.
[58] Nemat M, Lyons AC. An investigation of the surface topography of ball burnished mild steel and aluminium. Int J Adv Manuf Technol 2000;16:469–73.
[59] Klocke F, Backer V, Wegner H, Feldhaus B, Baron H, Hessert R. Influence of process and geometry parameters on the surface layer state after roller burnishing of IN718. Prod Eng Res Dev 2009;3:391–9.
[60] Nalla RK, Altenberger I, Noster U, Liu GY, Scholtes B, Ritchie RO. On the influence of mechanical surface treatments/deep rolling and laser shock peening on the fatigue behavior of

Please cite this article in press as: Revankar GD, et al. Wear resistance enhancement of titanium alloy (Ti–6Al–4V) by ball burnishing process. J Mater Res Technol. 2016. http://dx.doi.org/10.1016/j.jmrt.2016.03.007

Ti–6Al–4V at ambient and elevated temperatures. Mater Sci Eng A 2003;355:216–30.
[61] Prevéy PS, Hornbach DJ, Jacobs TL, Ravindranath R. Improved damage tolerance in titanium alloy fan blades with low plasticity burnishing. In: Proceedings of international surface engineering conference. 2002.
[62] Yasuhiro M, Kei D. Surface age hardening and wear properties of beta-type titanium alloy by laser surface solution treatment. Mater Trans 2011;52(4):714–8.
[63] Freese H, Volas MG, Wood JR. In: Brunette DM, Tengvall P, Textor M, Thomsen P, editors. Titanium in medicine. Berlin: Springer; 2001.
[64] Ohkubo C, Shimura I, Aoki T, Hanatani S, Hosoi T, Hattori M, et al. Wear resistance of experimental Ti–Cu alloys. Biomaterials 2003;24:3377–81.
[65] Chan KS, Koike M, Okabe T. Modeling wear of cast Ti alloys. Acta Biomater 2007;3:383–9.
[66] Gil FJ, Planell JA, Padrós A, Aparicio C. Effect of shot-blasting and heat treatment on fatigue fracture of titanium dental implants. Dental Mater 2007;23:486–91.
[67] López de Lacalle LN, Lamikiz A, Sánchez JA, Arana JL. The effect of ball burnishing on heat-treated steel and Inconel 718 milled surfaces. Int J Adv Manuf Technol 2007;32:958–68.
[68] Rigney DA. Some thoughts on sliding wear. Wear 1992;152:187–92.
[69] Hsu SM, Shen MC, Ruff AW. Wear prediction for metals. Tribol Int 1997;30:377–83.
[70] Suh NP. The delamination theory of wear. Wear 1973;25:111–24.
[71] Tan MJ, Zhu XJ. Dynamic recrystallization in commercially pure titanium. J Ach Mater Manuf Eng 2006;18:183–6.
[72] Wu X, Tao N, Hong Y, Liu G, Xu B, Lu J, et al. Strain-induced grain refinement of cobalt during surface mechanical attrition treatment. Acta Mater 2005;53(3):681–91.
[73] Altenberger I, Nalla RK, Yuji S, Lothar W, Ritchie RO. On the effect of deep-rolling and laser-peening on the stress-controlled low- and high-cycle fatigue behavior of Ti–6Al–4V at elevated temperatures up to 550 °C. Int J Fatigue 2012;44:292–302.
[74] Liu Y, Wang L, Wanga D. Finite element modeling of ultrasonic surface rolling process. J Mater Process Technol 2011;211:2106–13.
[75] Fischer-Cripps AC. Introduction to contact mechanics. 2nd ed. New York: Springer; 2007. p. 137–50.
[76] Farough M, Ramin S, Ali B. Finite element analysis and design optimization of low plasticity burnishing process. Int J Adv Manuf Technol 2014;70:1337–54.
[77] Sayahi M, Sghaier S, Belhadjsalah H. Finite element analysis of ball burnishing process: comparisons between numerical results and experiments. Int J Adv Manuf Technol 2013;67:1665–73.

Please cite this article in press as: Revankar GD, et al. Wear resistance enhancement of titanium alloy (Ti–6Al–4V) by ball burnishing process. J Mater Res Technol. 2016. http://dx.doi.org/10.1016/j.jmrt.2016.03.007